Article

Cell Reports

Diminished MTORC1-Dependent JNK Activation Underlies the Neurodevelopmental Defects Associated with Lysosomal Dysfunction

Graphical Abstract

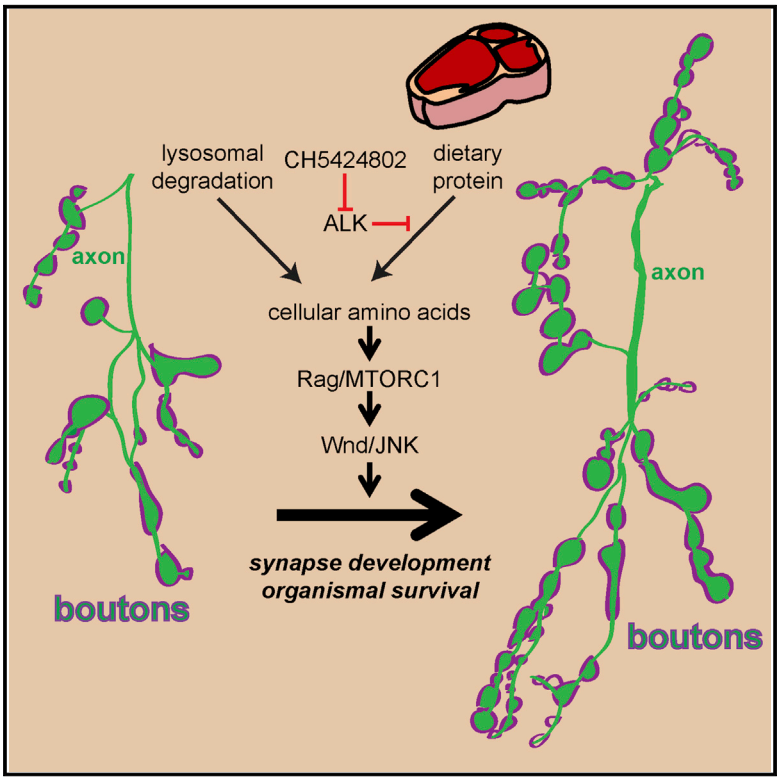

Authors

Ching- On Wong, Michela Palmieri, Jiaxing Li, ..., Catherine A. Collins, Marco Sardiello, Kartik Venkatachalam

Correspondence

kartik.venkatachalam@uth.tmc.edu

In Brief

Wong et al. identify an MTORC1-JNK signaling axis in *Drosophila* and mouse neurons required for synaptic development, which is attenuated upon endolysosomal dysfunction. The authors' findings suggest a possible therapeutic strategy that may be beneficial for tackling the neurodevelopmental defects commonly observed in lysosomal storage diseases with CNS involvement.

Highlights

- Fly models of lysosomal storage diseases (LSDs) exhibit diminished synaptic growth
- Lysosomal protein degradation and MTORC1 activation promote synaptic growth via JNK
- MTORC1 phosphorylates Wallenda/DLK1, an MAPKKK upstream of JNK in flies and mammals
- ALK inhibition along with high protein diet restores synaptic growth in LSD models

Wong et al., 2015, Cell Reports *12*, 2009–2020
September 29, 2015 ©2015 The Authors
http://dx.doi.org/10.1016/j.celrep.2015.08.047

CellPress

Cell Reports
Article

OPEN ACCESS
CellPress

Diminished MTORC1-Dependent JNK Activation Underlies the Neurodevelopmental Defects Associated with Lysosomal Dysfunction

Ching-On Wong,[1] Michela Palmieri,[2] Jiaxing Li,[3] Dmitry Akhmedov,[1] Yufang Chao,[1] Geoffrey T. Broadhead,[1] Michael X. Zhu,[1,4] Rebecca Berdeaux,[1,4] Catherine A. Collins,[3] Marco Sardiello,[2] and Kartik Venkatachalam[1,4,5,*]
[1]Department of Integrative Biology and Pharmacology, University of Texas School of Medicine, Houston, TX 77030, USA
[2]Department of Molecular and Human Genetics, Baylor College of Medicine, Jan and Dan Duncan Neurological Research Institute, Texas Children's Hospital, Houston, Texas, TX 77030, USA
[3]Department of Molecular, Cellular, and Developmental Biology, University of Michigan, Ann Arbor, MI 48109, USA
[4]Program in Cell and Regulatory Biology (CRB), Graduate School of Biomedical Sciences, University of Texas School of Medicine, Houston, TX 77030, USA
[5]Program in Neuroscience, Graduate School of Biomedical Sciences, University of Texas School of Medicine, Houston, TX 77030, USA
*Correspondence: kartik.venkatachalam@uth.tmc.edu
http://dx.doi.org/10.1016/j.celrep.2015.08.047
This is an open access article under the CC BY-NC-ND license (http://creativecommons.org/licenses/by-nc-nd/4.0/).

SUMMARY

Here, we evaluate the mechanisms underlying the neurodevelopmental deficits in *Drosophila* and mouse models of lysosomal storage diseases (LSDs). We find that lysosomes promote the growth of neuromuscular junctions (NMJs) via Rag GTPases and mechanistic target of rapamycin complex 1 (MTORC1). However, rather than employing S6K/4E-BP1, MTORC1 stimulates NMJ growth via JNK, a determinant of axonal growth in *Drosophila* and mammals. This role of lysosomal function in regulating JNK phosphorylation is conserved in mammals. Despite requiring the amino-acid-responsive kinase MTORC1, NMJ development is insensitive to dietary protein. We attribute this paradox to anaplastic lymphoma kinase (ALK), which restricts neuronal amino acid uptake, and the administration of an ALK inhibitor couples NMJ development to dietary protein. Our findings provide an explanation for the neurodevelopmental deficits in LSDs and suggest an actionable target for treatment.

INTRODUCTION

Mucolipidosis type IV (MLIV) and Batten disease are untreatable lysosomal storage diseases (LSDs) that cause childhood neurodegeneration (Vellodi, 2005; Venkatachalam et al., 2015). MLIV arises from loss-of-function mutations in the gene encoding TRPML1, an endolysosomal cation channel belonging to the TRP superfamily (Bargal et al., 2000; Bassi et al., 2000; Sun et al., 2000). The absence of TRPML1 leads to defective lysosomal storage and autophagy, mitochondrial damage, and macromolecular aggregation, which together initiate the protracted neurodegeneration observed in MLIV (Curcio-Morelli et al., 2010; Jennings et al., 2006; Miedel et al., 2008; Vergarajauregui and Puertollano, 2008). Batten disease arises from the absence of a lysosomal protein, CLN3 (Mitchison et al., 1997; Munroe et al., 1997), and results in psychomotor retardation (Kristensen and Lou, 1983). Both diseases cause early alterations in neuronal function. For instance, brain imaging studies revealed that MLIV and Batten patients display diminished axonal development in the cortex and corpus callosum (Autti et al., 1996; Frei et al., 1998), the causes of which remain unknown.

To better understand the etiology of MLIV in a genetically tractable model, we generated flies lacking the TRPML1 ortholog. The *trpml*-deficient (*trpml*^{1}) flies have helped us gain insight into the mechanisms of neurodegeneration and lysosomal storage (Venkatachalam et al., 2008, 2013; Wong et al., 2012). Here, we report that *trpml*^{1} larvae exhibit diminished synaptic growth at the NMJ, a well-studied model synapse (Collins and DiAntonio, 2007). We find that lysosomal function supports Rag GTPases and MTORC1 activation, and this is essential for JNK phosphorylation and synapse development. *Drosophila* larvae and mice lacking CLN3 also exhibit diminished Rag/MTORC1 and JNK activation, suggesting that alterations in neuronal signaling are similar in different LSDs and are evolutionarily conserved. Interestingly, the NMJ defects in the two fly LSD models were suppressed by the administration of a high-protein diet and a drug that is currently in clinical trials to treat certain forms of cancer. These findings inform a pharmacotherapeutic strategy that may suppress the neurodevelopmental defects observed in LSD patients.

RESULTS

Drosophila TRPML Is a Late-Endosomal/Lysosomal Protein in Neurons that Is Required for Synapse Development

In non-neuronal cells, TRPML shuttles between the plasma membrane and late-endosomal (LE) membranes (Wong et al., 2012). Here, we sought to evaluate the subcellular location of

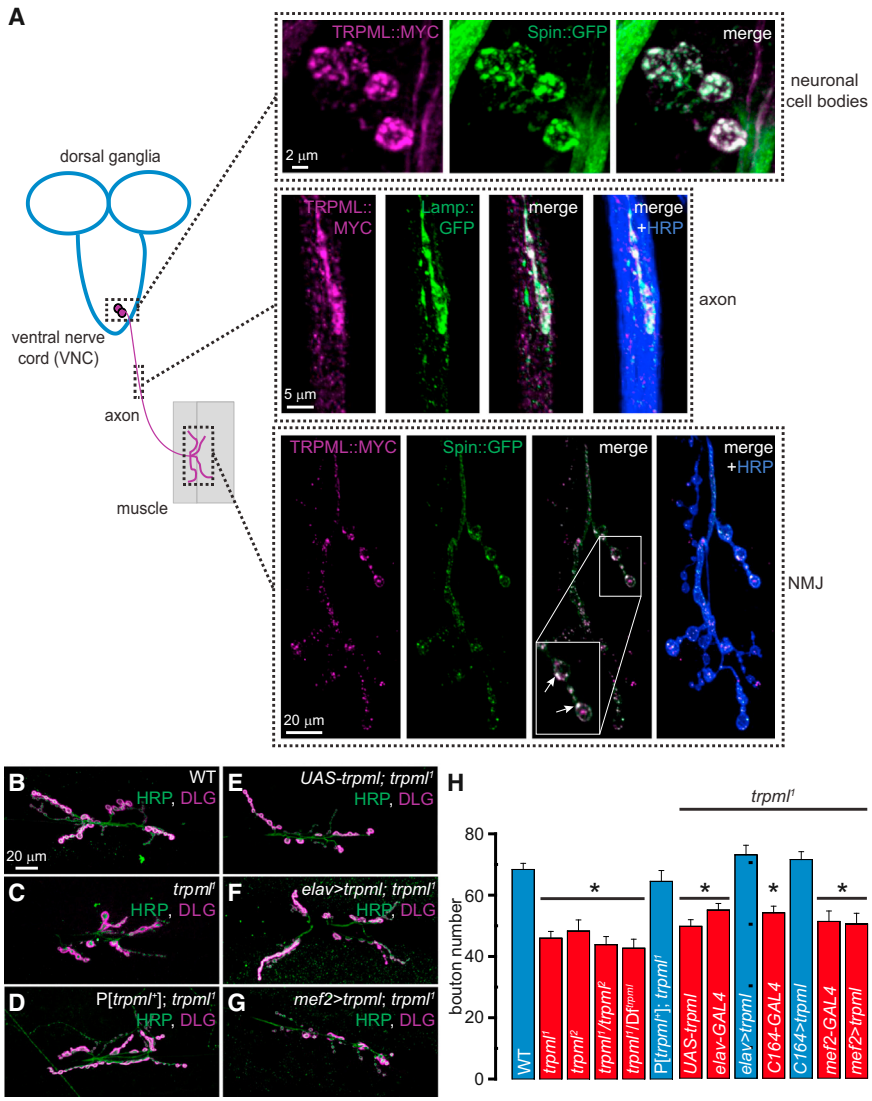

Figure 1. TRPML Is Required for Larval NMJ Development in *Drosophila*

(A) TRPML::MYC colocalizes with LE/lysosomal markers in neuronal cell bodies, axons, and NMJs. Image on the left shows *Drosophila* larval MNs, whose cell bodies reside in the VNC and project axons to peripheral muscles. Only one set of MNs, muscle, and NMJ is shown for simplicity. Images on the top right are confocal images of neuronal cell bodies in the larval VNC dissected from animals expressing TRPML::MYC (magenta) and Spin::GFP (green) in neurons. Scale bar shown in the left panel applies to all panels. Images in the middle are confocal images of larval axons in animals expressing TRPML::MYC (magenta) and Lamp::GFP (green) in neurons. Scale bar shown in the left panel applies to all panels. Images on the bottom right are confocal images of larval NMJs from animals expressing TRPML::MYC (magenta) and Spin::GFP (green) in neurons. α-Horseradish peroxidase (HRP, blue) primary antibodies were used to stain axonal membranes. Scale bar shown in the left panel applies to all panels.

(B–G) Confocal images of larval NMJs from animals of the indicated genotypes stained with primary antibodies against HRP (green) and DLG (magenta). Scale bar shown in (B) also applies to (C)–(G).

(H) Bar graph showing the average bouton numbers in larval NMJs from animals of the indicated genotypes.

* represents statistical significance. Data shown indicate mean ± SEM.

TRPML in neurons. The cell bodies of the *Drosophila* larval motor neurons (MNs) reside in the ventral nerve cord (VNC) and send axonal projections to the NMJs (Figure 1A). Coexpression of *UAS-trpml::myc* (TRPML::MYC) with the LE/lysosomal markers *UAS-spinster::gfp* (Spin::GFP) or *UAS-lamp::gfp*, using *elav*^{C155}*-GAL4* (*elav-GAL4*) revealed that TRPML::MYC colocalized with the LE/lysosomal markers within neuronal cell bodies, axons, and NMJs (Figure 1A).

We found that *trpml*-deficient larvae exhibited fewer NMJ boutons compared to wild-type (WT) (Figures 1B–1H). This phenotype was observed in the two loss-of-function alleles (*trpml*^{1} and *trpml*^{2}), the *trpml*^{1}/*trpml*^{2} transheterozygotes, and when the *trpml*^{1} allele was in *trans* with a deficiency uncovering the *trpml* locus (*trpml*^{1}/Df^{trpml}) (Figure 1H). The *trpml*^{1} NMJ growth phenotype was suppressed by a *trpml*$^{+}$ genomic rescue (P[*trpml*$^{+}$]; *trpml*^{1}) (Figures 1D and 1H). To identify the cells that require TRPML to promote NMJ growth, we selectively expressed *UAS-trpml* in *trpml*^{1} neurons or muscle. We found that expression of *UAS-trpml* in mutant neurons using *elav-GAL4* or the MN specific, *C164-GAL4*, rescued the NMJ growth defect (Figures 1E, 1F, and 1H). However, expression of *UAS-trpml* in *trpml*^{1} muscle using *mef2-GAL4* did not restore the bouton numbers (Figures 1G and 1H). Thus, loss of TRPML results in a presynaptic defect in MNs, leading to diminished NMJ growth.

Diminished Synaptic Growth in *trpml*^{1} Is Due to Decreased Activity of Rag GTPases/MTORC1

TRPML-dependent Ca^{2+} release allows the fusion of amphisomes with lysosomes, lysosomal degradation of proteins, and the production of free amino acids that activate Rag GTPases (Figure 2A) (Sancak et al., 2008; Wong et al., 2012). To address whether a decrease in Rag GTPase activation might underlie the diminished NMJ synaptic growth in *trpml*^{1}, we first examined NMJ growth in larvae lacking *ragC* (Kim et al., 2008). Compared to the heterozygous controls (*ragC*$^{\Delta}$/+), *ragC*-deficient larvae (*ragC*$^{\Delta}$) showed fewer NMJ boutons (Figures 2B, 2C, and 2H). Similarly, neuronal expression of a dominant-negative RagA (RagA^{TN}) decreased the bouton numbers (Figures 2D, 2E, and 2H). However, when expressed in *trpml*^{1} neurons, RagA^{TN} did not further decrease bouton numbers

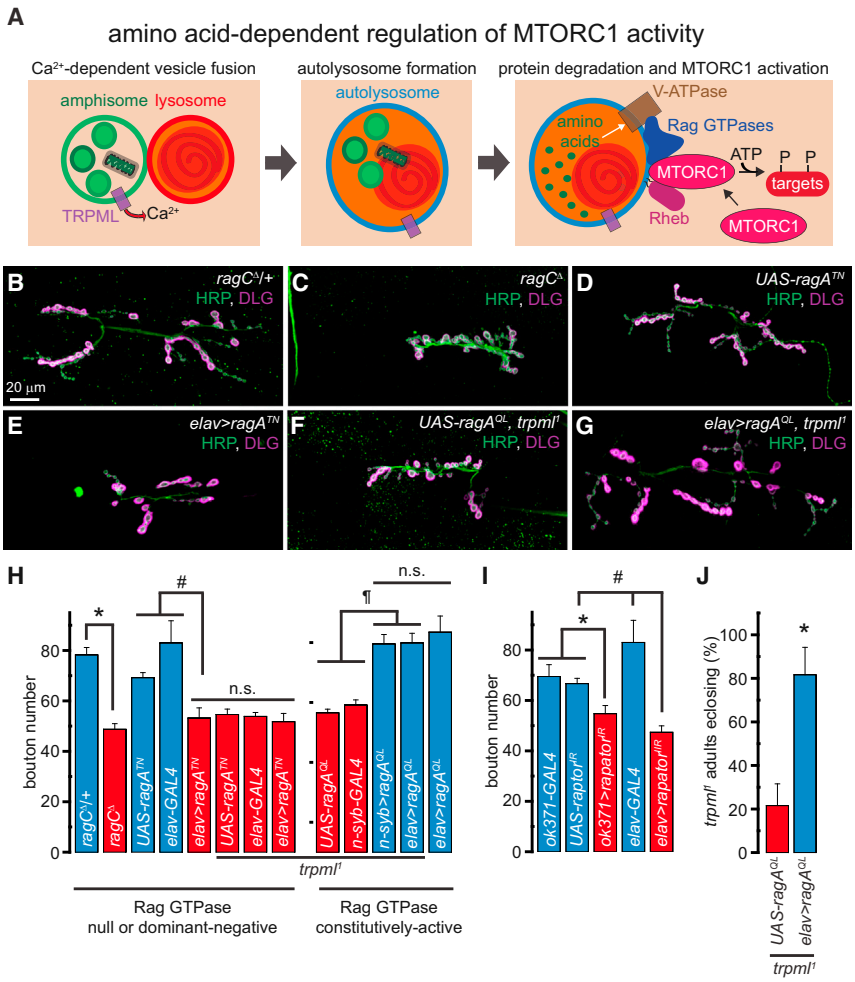

Figure 2. Diminished NMJ Synaptic Growth following Lysosomal Dysfunction Is Due to Decreased Activation of Rag/MTORC1

(A) TRPML is required for vesicle fusion, and MTORC1 is activated in the presence of lysosomal free amino acids, resulting in the phosphorylation of downstream targets.

(B–G) Confocal images of larval NMJs from animals of the indicated genotypes stained with antibodies against HRP (green) and DLG (magenta). Scale bar shown in (B) also applies to (C-G).

(H and I) Bar graphs showing the average bouton numbers in animals of the indicated genotypes.

(J) Bar graph showing the percentage of the *trpml*^{1} adults carrying the indicated transgenes that eclose from the pupal cases.

*, #, and ¶ represent statistical significance. Abbreviations: n.s., not significant. Data shown indicate mean ± SEM.

(Figure 2H). This lack of additivity suggests that Rag and TRPML function in a common pathway responsible for NMJ development. Indeed, expression of a constitutively active RagA (RagA^{QL}) in *trpml*^{1} neurons completely rescued the synaptic growth defects (Figures 2F–2H). However, expression of *ragA*^{QL} in WT neurons did not lead to an increase in bouton numbers (Figure 2H), indicating that the rescue of the *trpml*^{1} phenotype by RagA^{QL} occurred by counteracting a decrease in Rag activity and not by some unrelated effects of RagA^{QL} expression.

Rag GTPases are required for the function of MTORC1 (Sancak et al., 2008). Because Rag GTPases play a role in *Drosophila* NMJ development, we asked whether MTORC1 also plays a role in this process. We knocked down the critical MTORC1 subunit, Raptor (Hara et al., 2002), using an RNAi line (*raptor*^{JR}), which has been shown to lower *raptor* mRNA levels and MTORC1 activity (Natarajan et al., 2013). Consistent with the previously published effects of this RNAi line on MTORC1 activity, we observed decreased pS6K in fat-body extracts from larvae expressing the *raptor*^{JR} using *cg-GAL4* (Figure S1A). Moreover, expression of *UAS-raptor*^{JR} in MNs using *vglut*^{ok371}*-GAL4* (*ok371-GAL4*) or in all neurons resulted in fewer boutons (Figure 2I). Therefore, activities of both Rag and MTORC1 are required for NMJ development.

The *trpml*^{1} mutants exhibit late-pupal lethality (only 10%–20% of *trpml*^{1} pharate adults eclose), which can be partially suppressed by feeding the mutant larvae a protein-rich diet (allowing ~50% of *trpml*^{1} pharate adults to eclose) (Wong et al., 2012). Expression of RagA^{QL} in *trpml*^{1} neurons allowed ~80% of the pharate adults to eclose even without the administration of a high-protein diet (Figure 2J). Therefore, the decrease in Rag activity in *trpml*^{1} neurons underlies both the synaptic growth defects and elevated pupal lethality. Moreover, rescue of both synaptic growth defects and pupal lethality by RagA^{QL} suggest a common molecular origin for the disparate *trpml*^{1} phenotypes.

The Rag-Ragulator complex activates MTORC1 in response to an increase in amino acid levels (Bar-Peled et al., 2012) or a decrease in the activity of AMPK (Zhang et al., 2014) (Figure S1B). AMPK inhibits MTORC1 via phosphorylation and activation of the TSC1/TSC2 complex, which is a GAP for Rheb, a G protein required for MTORC1 function (Zoncu et al., 2011). To evaluate a role for AMPK in the *trpml*^{1} NMJ phenotypes, we expressed either constitutively active or dominant-negative AMPK (AMPK^{T184D} or AMPK^{K56R}, respectively; Figure S1B) in WT and *trpml*^{1} neurons. Although neuronal expression of AMPK^{T184D} results in diminished bouton numbers, expression of AMPK^{T184D} in *trpml*^{1} did not further decrease bouton numbers (Figure S1C). These data are consistent with Rag GTPases being inhibited to a similar extent by the absence of TRPML or an increase in AMPK activity. However, expression of AMPK^{K56R} in *trpml*^{1} neurons did not restore bouton numbers (Figure S1C). Thus, compromised activities of Rag GTPases in *trpml*^{1} neurons are not due to AMPK overactivation but likely reflect lower cellular amino acid levels due to diminished lysosomal protein degradation.

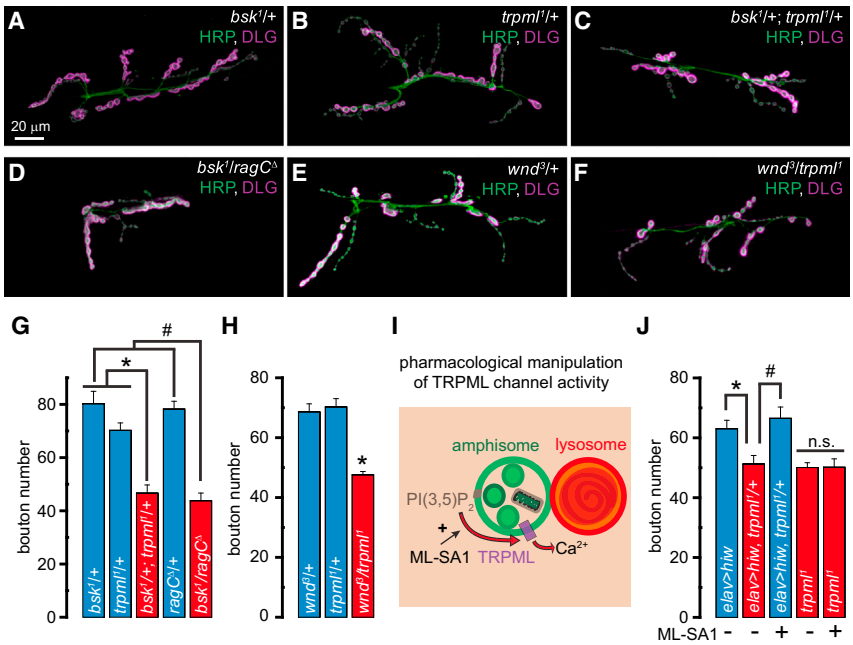

Figure 3. *trpml* and *ragC* Exhibit Dominant Genetic Interactions with Genes Encoding Proteins Involved in MAP Kinase Signaling

(A–F) Confocal images of larval NMJs from animals of the indicated genotypes stained with antibodies against HRP (green) and DLG (magenta). Scale bar shown in (A) also applies to (B)–(F).

(G and H) Bar graphs showing the average bouton numbers in animals of the indicated genotypes.

(I) PI(3,5)P_2 activates TRPML, leading to vesicular Ca^{2+} release, and ML-SA1 potentiates this effect.

(J) Bar graph showing the average bouton numbers in animals of the indicated genotypes reared on instant food with or without ML-SA1 feeding as indicated. Rearing larvae on instant food resulted in an overall increase in the number of boutons in all the genotypes (Wong et al., 2014). However, the *trpml*^{1} mutants still showed a relative decrease in NMJ boutons, and all comparisons were made between animals reared under identical conditions.

* and # represent statistical significance. Abbreviations: n.s., not significant. Data shown indicate mean ± SEM.

MTORC1-Dependent NMJ Development Is Independent of S6K and 4E-BP1

MTORC1-dependent phosphorylation activates S6K and inhibits 4E-BP1 (Zoncu et al., 2011). However, previous studies have reported that neither S6K nor 4E-BP1 (Thor) determines NMJ bouton numbers (Cheng et al., 2011a; Lee et al., 2010). We also found that neuronal expression of neither dominant-negative S6K nor wild-type Thor (*elav* > *S6K*^{KQ} and *elav>thor* respectively) altered NMJ bouton numbers (Figure S1D).

The efficacy of rapamycin on MTORC1 activity depends on the phosphorylation target. Although effective at inhibiting phosphorylation of S6K and 4E-BP1, rapamycin does not effectively inhibit phosphorylation of some other MTORC1 targets (Kang et al., 2013). Because S6K and 4E-BP1 do not impact NMJ bouton numbers, we hypothesized that NMJ growth might be resistant to rapamycin. Indeed, synaptic overgrowth following overexpression of Rheb is not suppressed by rapamycin (Knox et al., 2007). We also found that feeding WT larvae 1 μM rapamycin, a concentration that effectively inhibits MTORC1 activity in larval fat bodies (Wong et al., 2012), did not alter NMJ bouton numbers (Figure S1E). Together, these findings indicate that MTORC1 regulates NMJ growth via a target(s) other than S6K and 4E-BP1 (Figure S1F).

TRPML, Rag, and MTORC1 Promote NMJ Synapse Development via JNK

To identify the downstream target(s) of Rag/MTORC1 that impact(s) NMJ bouton numbers, we examined the pathways that influence NMJ synapse development in *Drosophila* larvae. The BMP/TGF-β retrograde cascade involves the phosphorylation of the transcription factor MAD, which promotes NMJ growth (Marqués et al., 2002; Sweeney and Davis, 2002). However, the relative intensities of pMAD staining at the NMJ and the MN nuclei were unchanged in *trpml*^{1} (Figures S2A–S2D), indicating that the diminished synaptic growth in *trpml*^{1} is not due to decreased BMP/TGF-β signaling. Mutants lacking a *Drosophila* Wnt homolog, Wingless (Wg), or exhibiting destabilized presynaptic microtubules have enlarged but fewer boutons (Miech et al., 2008; Packard et al., 2002; Pennetta et al., 2002; Roos et al., 2000; Wong et al., 2014). Although *trpml*^{1} displayed a decrease in bouton numbers, bouton morphology was not altered (Figures 1B–1G). Furthermore, the levels of presynaptic Wg remained unchanged in *trpml*^{1} (Figure S2E), suggesting that Wg release is not affected in *trpml*^{1}. Therefore, the *trpml*^{1} synaptic growth defects do not result from diminished Wg signaling or from alterations in presynaptic microtubule structure.

Next, we investigated whether presynaptic JNK signaling, which promotes NMJ development (Ballard et al., 2014; Sanyal et al., 2002), may be decreased in *trpml*^{1}. To do so, we first examined whether *trpml*^{1} exhibits dominant genetic interactions with loss-of-function mutations in JNK-related genes. Although larvae carrying single copies of *trpml*^{1} or the loss-of-function allele of *Drosophila* JNK (*basket*^{1} (*bsk*^{1})) did not exhibit a decrease in bouton numbers, transheterozygous *bsk*^{1}/+; *trpml*^{1}/+ NMJs showed fewer boutons (Figures 3A–3C and 3G). We also observed a dominant genetic interaction between *bsk*^{1} and *ragC*$^{\Delta}$ (Figures 3D and 3G). The MAPKKK Wallenda (Wnd), which is the *Drosophila* homolog of DLK1, is responsible for the activation of JNK in *Drosophila* MNs (Collins et al., 2006). Transheterozygous *wnd*^{3}/*trpml*^{1} NMJs also exhibited fewer synaptic boutons, whereas neither heterozygous alone showed the phenotype (Figures 3E, 3F, and 3H).

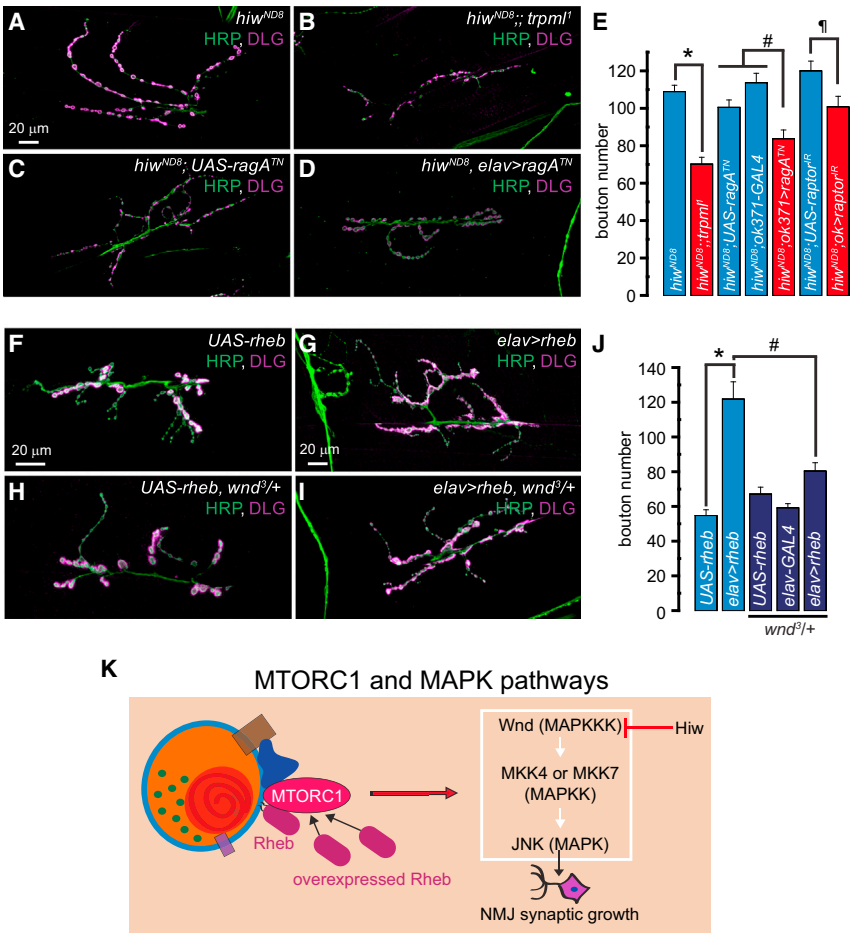

Figure 4. Lysosomal Function and Rag/MTORC1 Promote NMJ Synapse Growth via Wnd/JNK Signaling

(A–D) Confocal images of larval NMJs from animals of the indicated genotypes stained with antibodies against HRP (green) and DLG (magenta). Scale bar shown in (A) also applies to (B)–(D).

(E) Bar graph showing the average bouton numbers in animals of the indicated genotypes.

(F–I) Confocal images of larval NMJs from animals of the indicated genotypes stained with antibodies against HRP (green) and DLG (magenta). Scale bar shown in (F) also applies to (H), and scale bar shown in (G) also applies to (I).

(J) Bar graph showing the average bouton numbers in animals of the indicated genotypes.

(K) Crosstalk between the MTORC1 and Wnd/JNK pathways.

*, #, and ¶ represent statistical significance. Data shown indicate mean ± SEM.

The E3-ubiquitin ligase, Highwire (Hiw), restricts NMJ bouton numbers by promoting Wnd degradation (Collins et al., 2006). Neuronal expression of *UAS-hiw* in *trpml*^{1}/+ (*elav>hiw*; *trpml*^{1}/+) resulted in a decrease in bouton numbers that was not observed when *UAS-hiw* was expressed in WT neurons (*elav>hiw*) (Figure 3J). Therefore, *trpml*^{1}/+ neurons constitute a sensitized system in which expression of a negative regulator of JNK signaling restricts the formation of synaptic boutons. Interestingly, expression of Hiw in the *trpml*^{1} homozygotes resulted in synthetic embryonic lethality (not shown), likely due to massive downregulation of JNK signaling, because *bsk*^{1} homozygotes also exhibit embryonic lethality (Riesgo-Escovar et al., 1996).

Because the *elav>hiw; trpml*^{1}/+ still contained one functional copy of *trpml*, we asked whether exogenously activating TRPML in these animals would restore the bouton numbers. Both mammalian TRPML1 and fly TRPML are PI(3,5)P_2-activated channels (Dong et al., 2010; Feng et al., 2014a) whose activity is further potentiated by ML-synthetic agonist 1 (ML-SA1) (Feng et al., 2014b; Shen et al., 2012) (Figure 3I). Feeding ML-SA1 (20 μM final concentration in fly food) to the *elav>hiw*; *trpml*^{1}/+ larvae restored synaptic growth, whereas the *trpml*^{1} homozygous larvae were insensitive to ML-SA1 (Figure 3J). Thus, TRPML channel activity supports JNK-dependent NMJ growth.

Synaptic Overgrowth in *hiw*-Deficient Larvae Is Suppressed by Lysosomal Dysfunction or a Decreased Rag/MTORC1 Activity

Larvae lacking *hiw* (*hiw*^{ND8}) exhibit an elevated number of relatively smaller NMJ boutons (DiAntonio et al., 2001; Wan et al., 2000). Because decreasing JNK levels in *hiw*^{ND8} suppresses the alterations in synaptic growth and morphology (Collins et al., 2006), we hypothesized that *trpml*^{1} might also suppress the *hiw*^{ND8}-induced synaptic phenotypes. Indeed, *hiw*^{ND8};;*trpml*^{1} double mutants had significantly fewer boutons than *hiw*^{ND8} alone (Figures 4A, 4B, and 4E). The bouton numbers observed in *hiw*^{ND8} were also reduced following MN-specific expression of dominant-negative *ragA*^{TN} or *raptor*^{IR} (Figures 4C–4E). Thus, lysosomal function and Rag/MTORC1 activity are partially required for the NMJ synapse expansion in *hiw*^{ND8}, further supporting the notion that lysosomal function and Rag/MTORC1 are required for maximal JNK activation. However, none of the manipulations described above rescued the "small-bouton" phenotype of *hiw*^{ND8}.

Synaptic Overgrowth due to Rheb Overexpression Is Suppressed by *wnd* Mutants

Could the synaptic overgrowth associated with the neuronal overactivation of MTORC1 be suppressed by decreasing the levels of Wnd? As described previously (Knox et al., 2007; Natarajan et al., 2013), neuronal overexpression of Rheb (*elav>rheb*), which induces MTORC1 activation (Stocker et al., 2003) (Figure 4K), resulted in a 2-fold increase in the number of synaptic boutons (Figures 4F, 4G, and 4J). Interestingly, *wnd*^{3}/+ markedly suppressed the increase in bouton numbers in *elav>rheb* (Figures 4H–4J). Therefore, NMJ overgrowth following MTORC1 overactivation requires Wnd (Figure 4K).

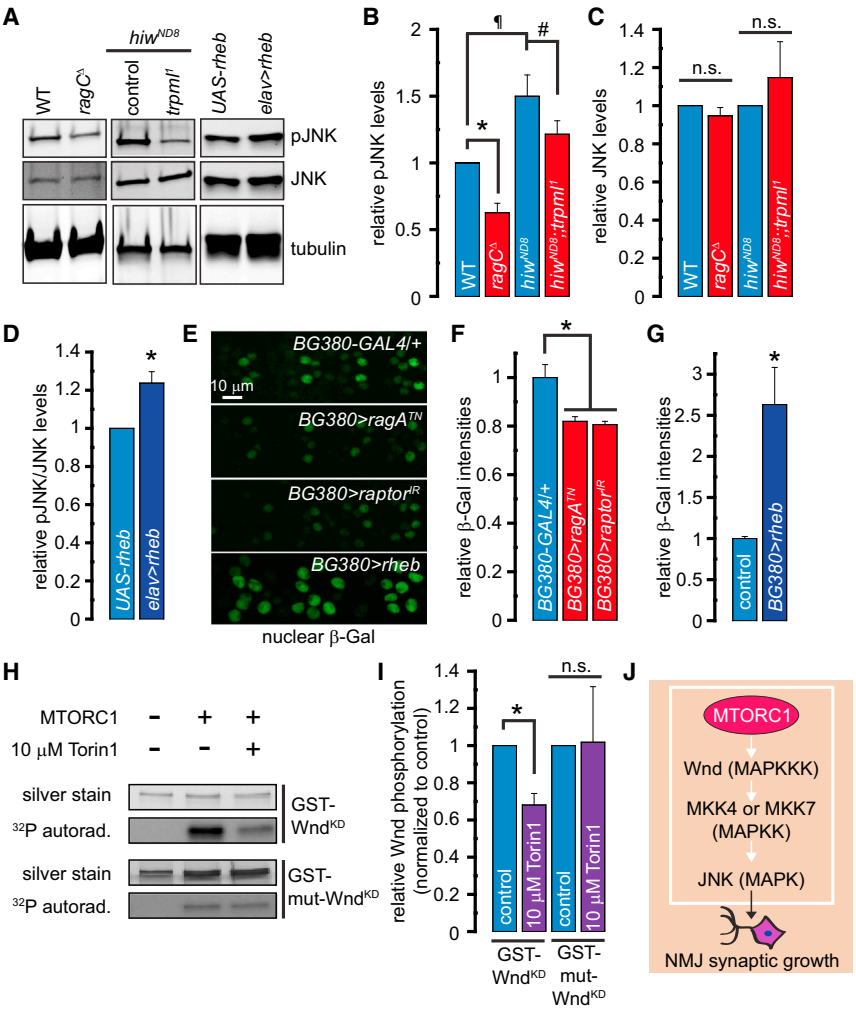

Figure 5. Lysosomal Function and Rag/MTORC1 Promote Wnd/JNK Phosphorylation and *puckered* Expression

(A) Western blots performed with larval brain extracts of the indicated genotypes probed with α-pJNK, α-JNK, and α-tubulin primary antibodies.

(B) Bar graph showing the pJNK band intensities normalized to the tubulin band intensities in the indicated genotypes.

(C) Bar graph showing the JNK band intensities normalized to the tubulin band intensities in the indicated genotypes.

Values shown in (B) and (C) are relative to the WT controls.

(D) Bar graph showing the pJNK/JNK band intensities in the indicated genotypes. The values shown are normalized to the *UAS-rheb* controls.

(E) Representative images showing nuclear β-gal staining in MN cell bodies in animals of the indicated genotypes. All animals shown in (E) carried the *puc-LacZ* transgene and *UAS-Dicer2*. *UAS-Dicer2* alone did not affect *puc-LacZ* expression (data not shown). The scale bar shown in the top panel applies to all panels. The *BG380>rheb* nuclei are larger consistent with the well-known effects of Rheb to increase cells size in *Drosophila* (Stocker et al., 2003), and the data shown are the average β-gal intensities over the entire nucleus to control for changes in nuclear size.

(F and G) Bar graph showing relative nuclear β-gal intensities in the indicated genotypes. The control in (G) is *BG380-GAL4/+*.

(H) In vitro kinase assay using purified MTORC1 on recombinant GST-Wnd^{KD} and GST-mut-Wnd^{KD}. Top: silver stain showing total GST-Wnd^{KD} or GST-mut-Wnd^{KD} levels in each sample. Bottom: ^{32}P autoradiograms showing extent of GST-Wnd^{KD} or GST-mut-Wnd^{KD} phosphorylation in the presence of purified MTORC1 with or without 10 μM Torin1 as indicated.

(I) Bar graph showing quantification of GST-Wnd^{KD} and GST-mut-Wnd^{KD} phosphorylation in the absence (control) or presence of 10 μM Torin1 as indicated. Data shown are normalized to controls.

(J) MTORC1 phosphorylates Wnd resulting in JNK activation and NMJ synaptic growth. MKK4 and MKK7 are MAPKK upstream of JNK (Geuking et al., 2009).

*, #, and ¶ represent statistical significance. Abbreviations: n.s., not significant. Data shown indicate mean ± SEM.

Rag/MTORC1 Activity Promotes JNK Phosphorylation and JNK-Dependent Gene Transcription

Next, we asked whether manipulation of the Rag/MTORC1 pathway impacts JNK phosphorylation. Western blotting of larval brain extracts revealed that the levels of phospho-JNK (pJNK) were significantly decreased in the *ragC*$^{\Delta}$ (Figures 5A and 5B). Consistent with increased Wnd levels in *hiw*^{ND8} mutants (Collins et al., 2006), pJNK levels were elevated in the *hiw*^{ND8} larval brain extracts (Figures 5A and 5B). The pJNK elevation in *hiw*^{ND8} was significantly reduced following the introduction of *trpml*^{1} (Figures 5A and 5B). However, the total JNK levels were not altered in these genotypes (Figures 5A and 5C). Conversely, the levels of pJNK/JNK were elevated in brain extracts derived from *elav>rheb* larvae (Figures 5A and 5D). Therefore, JNK phosphorylation correlates with MTORC1 activity.

The gene *puckered* (*puc*) is expressed following JNK activation (Martín-Blanco et al., 1998), and the *puc-LacZ* reporter is used to assess JNK-dependent gene transcription (Rämet et al., 2002). Although we were unable to recombine the *puc-LacZ* transgene with *trpml*^{1}, we monitored nuclear β-galactosidase (β-gal) staining intensities in larvae carrying the *puc-LacZ* transgene, in which either dominant-negative *ragA*^{TN} or *raptor*^{IR} were expressed under the control of the MN-specific, *BG380-GAL4*. We found that expression of *ragA*^{TN} or *raptor*^{IR} significantly decreased β-gal intensities, i.e., *puc-LacZ* induction (Figures 5E and 5F). However, expression of an RNAi against *moody*, a gene unrelated to the MTORC1 pathway, did not alter the β-gal intensity (β-gal intensity relative to *BG380-GAL4/+* = 0.98, p = 0.8, unpaired Student's t test). Expression of *UAS-rheb* under the control of *BG380-GAL4* led to a 2.5-fold increase in β-gal intensity (Figures 5E and 5G). Therefore, JNK-dependent transcription correlates with MTORC1 activity.

MTORC1 Phosphorylates Wnd

Evaluation of the primary amino acid sequence of Wnd revealed that although the protein contains a total of 69 serine and 8

threonine residues that can be phosphorylated (NetPhos2.0), only 4 of these sites bear the hallmarks of MTOR consensus sites (S305, T309, S362, and S392) (Hsu et al., 2011). To test the hypothesis that MTORC1 phosphorylates Wnd at one or more of these residues, we first purified MTORC1 from cells stably expressing FLAG-tagged Raptor (FLAG-Raptor) (Yip et al., 2010). Both MTOR and FLAG-Raptor were present in the purified complex, along with the kinase ULK1/Atg1, which interacts with MTORC1 (Hosokawa et al., 2009) (Figure S3A). In contrast, JNK was absent in the purified complex, whereas it was detected in both the input and flow-through (Figure S3A). The MTORC1 complex we purified was functional as it phosphorylated recombinant 4E-BP1 in vitro (Figure S3B), and this phosphorylation was abolished by the MTOR kinase inhibitor Torin1 (Thoreen et al., 2009) (Figure S3B).

Next, we purified a glutathione S-transferase (GST)-tagged kinase-dead Wnd (GST-Wnd^{KD}—K188A, to rule out autophosphorylation of Wnd) from *E. coli* and evaluated its phosphorylation by MTORC1 in vitro (Stewart et al., 2013). We found that GST-Wnd^{KD} was phosphorylated only in the presence of MTORC1, and Torin1 significantly decreased this phosphorylation (Figures 5H and 5I). However, GST alone was not phosphorylated by MTORC1 (Figure S3C). Interestingly, the phosphorylation of GST-Wnd^{KD} was only decreased by ~30% following Torin1 treatment, which indicates that the MTORC1 we purified also contains Torin1-insensitive kinase(s) that can phosphorylate GST-Wnd^{KD}. Consistent with this notion, although GST-Wnd^{KD} lacking the four putative MTOR phosphorylation sites (GST-mut-Wnd^{KD}; contains the following mutations: K188A, S305A, T309A, S362A, and S392A) was phosphorylated by MTORC1, this residual phosphorylation was insensitive to Torin1 (Figures 5H and 5I). Therefore, Torin1-sensitive phosphorylation of GST-Wnd^{KD} by MTORC1 occurs at the four predicted MTOR target sites, whereas additional kinase(s) in the complex phosphorylate(s) Wnd on other phosphorylation sites in the protein. Our data indicate that MTORC1 directly phosphorylates Wnd, which stimulates JNK phosphorylation and promotes NMJ growth (Figure 5J).

Diminished NMJ Bouton Numbers, Rag/MTORC1 Activation, and JNK Activation Are Also Observed in a *Drosophila* Model of Batten Disease

To examine whether decreased neuronal JNK signaling is a general outcome of lysosomal dysfunction, we first examined JNK phosphorylation in larvae that were fed chloroquine, a lysosomotropic agent that disrupts lysosomal degradation of proteins. Chloroquine-fed larvae exhibited a significant decrease in pJNK/JNK levels in the brain (Figures S4A and S4B). Thus, decreased lysosomal protein degradation results in diminished JNK phosphorylation.

Next, we sought to evaluate synaptic development and JNK signaling in flies lacking *cln3*. Similar to our findings in *trpml^{1}*, the number of NMJ boutons in *cln3*-deficient larvae (*cln3$^{\Delta MB1}$*) (Tuxworth et al., 2009) was significantly lower than those in heterozygous controls (*cln3$^{\Delta MB1}$*/+) (Figures 6A–6C). We also expressed an RNAi line against *Drosophila cln3* (*UAS-cln3^{IR}*) in MNs and observed a decrease in the number of synaptic boutons (Figures S3C, S3D, and 6C). Therefore, loss of either *trpml* or *cln3* in MNs results in diminished synaptic growth at the NMJ, indicating a general role of lysosomal function in synaptic development.

The *trpml^{1}* and *cln3$^{\Delta MB1}$* mutants exhibited dominant genetic interactions, whereas bouton numbers in the *cln3$^{\Delta MB1}$*/+ and *trpml^{1}*/+ heterozygotes alone remained unchanged (Figure 6D), and expression of RagA^{QL} in the *cln3$^{\Delta MB1}$* resulted in complete restoration of bouton numbers (Figure 6D). Furthermore, neuronal expression of *UAS-cln3^{IR}* led to lower levels of pJNK (Figures 6E and 6F), but not total JNK (data not shown), and a significant decreased bouton numbers in *hiw^{ND8}* (Figures S3E–S3G). Therefore, diminished synaptic bouton numbers in both *trpml^{1}* and *cln3$^{\Delta MB1}$* occur via a similar pathway involving low Rag/MTORC1 activity and JNK phosphorylation.

Neuronal JNK Phosphorylation Is Diminished in a Mouse Model of Batten Disease

JNK activation is required for axonal tract development in the corpus callosum (CC) and cortex in mice (Eto et al., 2010). Brain sections from embryonic day 19.5 (E19.5) embryos revealed lower pJNK levels in the CC in the *Cln3*-deficient animal (*Cln3$^{\Delta 7\text{-}8/\Delta 7\text{-}8}$*, hereafter referred to as *Cln3$^{-/-}$*) (Cotman et al., 2002) (Figures 6G–6L). The decrease in pJNK levels in the *Cln3$^{-/-}$* axons was particularly striking in the commissures adjacent to the CC (Figures 6H and 6J–6L, compare regions indicated by arrows in the two genotypes). However, the total JNK levels were not changed in the *Cln3$^{-/-}$* sections (Figures S3H–S3K). Cerebral cortex lysates from E17.5 *Cln3$^{-/-}$* mice embryos also exhibited significantly reduced levels of pJNK and ratio of pJNK/JNK (Figures 6M–6O). Thus, decreased neuronal JNK activation following lysosomal dysfunction occurs in multiple LSD models and is conserved between flies and mammals.

Simultaneous Inhibition of ALK and Administration of High-Protein Diet Partially Rescue the *trpml^{1}* Synaptic Growth Defects and Pupal Lethality

Feeding *trpml^{1}* larvae a high-protein diet promotes the activation of Rag and suppresses the mutant phenotypes in non-neuronal cells (Wong et al., 2012). Because the NMJ growth defects in *trpml^{1}* also arise from a decrease in the activity of Rag, we examined whether feeding *trpml^{1}* larvae a high-protein diet could rescue the synaptic growth defects. To our surprise, we found that raising the *trpml^{1}* larvae on a high-protein diet did not affect the NMJ growth defects (Figure 7A). Therefore, although *trpml^{1}* neurons exhibit decreased activation of an amino-acid-responsive cascade, these cells are unable to adequately respond to an elevation in dietary protein content.

These data were consistent with previous findings that *Drosophila* neuroblasts are insensitive to dietary protein content compared to non-neuronal cells (Cheng et al., 2011b). This insensitivity is due to the evolutionarily conserved receptor-tyrosine kinase ALK, which is enriched in neurons and represses neuronal amino acid uptake (Figure 7B, left and middle), while promoting neuroblast development by activating phosphatidylinositol 3-kinase (PI3K), thereby allowing neuroblasts to withstand fluctuations in dietary amino acids (Cheng et al., 2011b) (Figure 7B, middle). Owing to the expression of ALK in mature neurons (Rohrbough et al., 2013), amino acid uptake might remain suppressed in these cells. If so, inhibition of ALK in

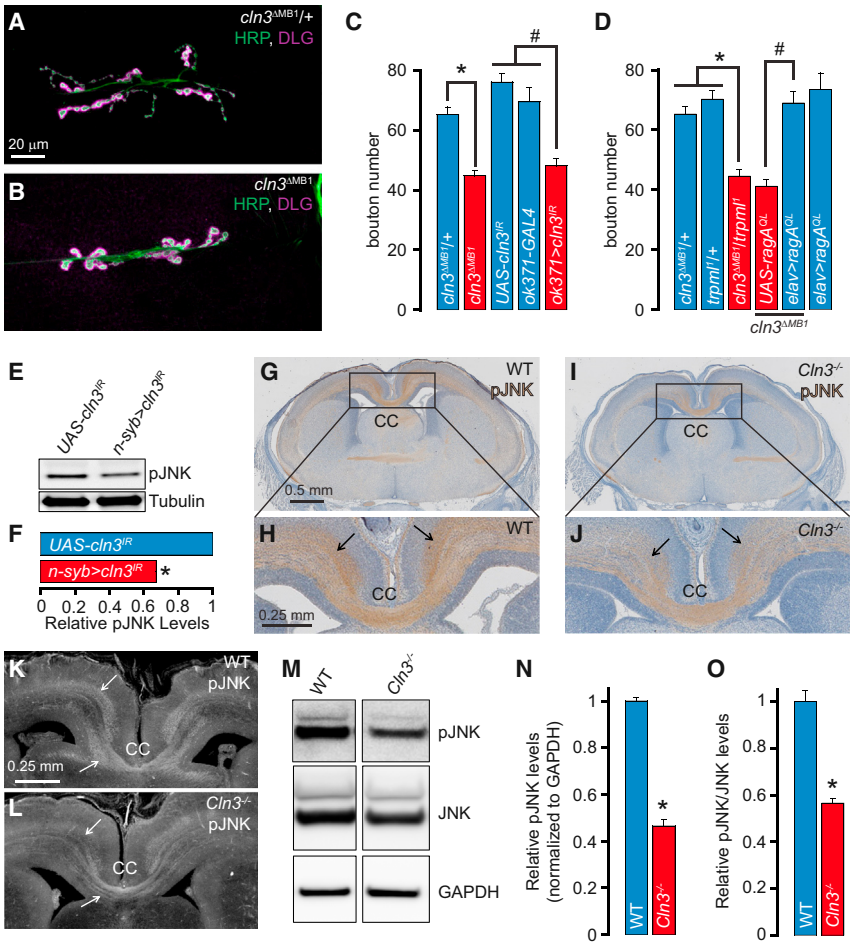

Figure 6. *Drosophila* and Mouse Models of Batten Disease Also Show Diminished Neuronal JNK Signaling

(A and B) Confocal images of larval NMJs from animals of the indicated genotypes stained with antibodies against HRP (green) and DLG (magenta). Scale bar shown in (A) also applies to (B).

(C and D) Bar graphs showing the average bouton numbers in animals of the indicated genotypes.

(E) Western blots performed with larval brain extracts of the indicated genotypes probed with α-pJNK and α-tubulin primary antibodies.

(F) Bar graph showing the pJNK band intensities normalized to the tubulin band intensities in the indicated genotypes. The values shown are relative to the appropriate *UAS* controls.

(G and I) Coronal sections of E19.5 mouse brains of the indicated genotypes showing α-pJNK staining by immunohistochemistry. Scale bar shown in (G) also applies to (I).

(H and J) Higher magnification of the boxed regions from (G) and (I), respectively. Scale bar shown in (H) also applies to (J).

(K and L) Coronal sections of E19.5 mouse brains of the indicated genotypes showing α-pJNK staining by immunofluorescence. Scale bar shown in (K) also applies to (L).

Arrows in (H) and (J)–(L) point to α-pJNK staining in axonal tracts.

(M) Western blots performed with cerebral cortex lysates from animals of the indicated genotypes probed with α-pJNK, α-JNK, and α-GAPDH primary antibodies.

(N and O) Bar graph showing the relative pJNK band intensities normalized to the GAPDH band intensities in the indicated genotypes (N) and the relative pJNK/JNK band intensities in the indicated genotypes (O). The values shown are relative to the appropriate controls.

* represents statistical significance. Abbreviations: n.s., not significant; CC, corpus callosum. Data shown indicate mean ± SEM.

trpml^{1} could derepress the uptake of dietary amino acids, resulting in the activation of Rag and recovery of synaptic growth (Figure 7B, right).

We tested this hypothesis by feeding larvae a highly selective ALK inhibitor, CH5424802 (Sakamoto et al., 2011). The amino acid residues on ALK that mediate the effect of CH5424802 are conserved in *Drosophila* ALK. Moreover, CH5424802 treatment resulted in decreased phosphorylation of Akt on S473 (Figures S4L and S4M), a known consequence of inhibition of ALK, which is responsible for phosphorylation of Akt on S473 via PI3K (Slupianek et al., 2001). Next, we fed larvae CH5424802 (final concentration of 1 μM in fly food) either with or without a high-protein diet for ~48 hr. Remarkably, only the *trpml*^{1} larvae that were fed both CH5424802 and a high-protein diet showed significant recovery of the synaptic bouton numbers (Figure 7C). However, the combination of a high-protein diet and CH5424802 did not elevate the bouton numbers when either dominant-negative *ragA*^{TN} was simultaneously expressed in the *trpml*^{1} neurons (Figure 7C) or in *ragC*$^{\Delta}$ (Figure 7D). We also observed significant rescue of bouton numbers in larvae expressing *cln3* RNAi in MNs following simultaneous administration of CH5424802 and high-protein diet (Figure 7E). Thus, inhibition of ALK is critical for restoration of Rag activity and synaptic growth by a high-protein diet in neurons with lysosomal dysfunction.

Feeding the *trpml*^{1} larvae a combination of yeast and CH5424802 also significantly increased the percentage of flies surviving to adulthood compared to feeding the larvae a diet comprised of yeast without CH5424802 (Figure 7F). Therefore, a combination of a high-protein diet and ALK inhibition rescues defects in both synapse development and adult viability in animals with lysosomal dysfunction.

DISCUSSION

Lysosomal Dysfunction Results in Diminished Synapse Development

We show that lysosomal dysfunction in *Drosophila* MNs results in diminished bouton numbers at the larval NMJ. We present evidence that lysosomal dysfunction results in decreased activation of the amino-acid-responsive cascade involving Rag/MTORC1,

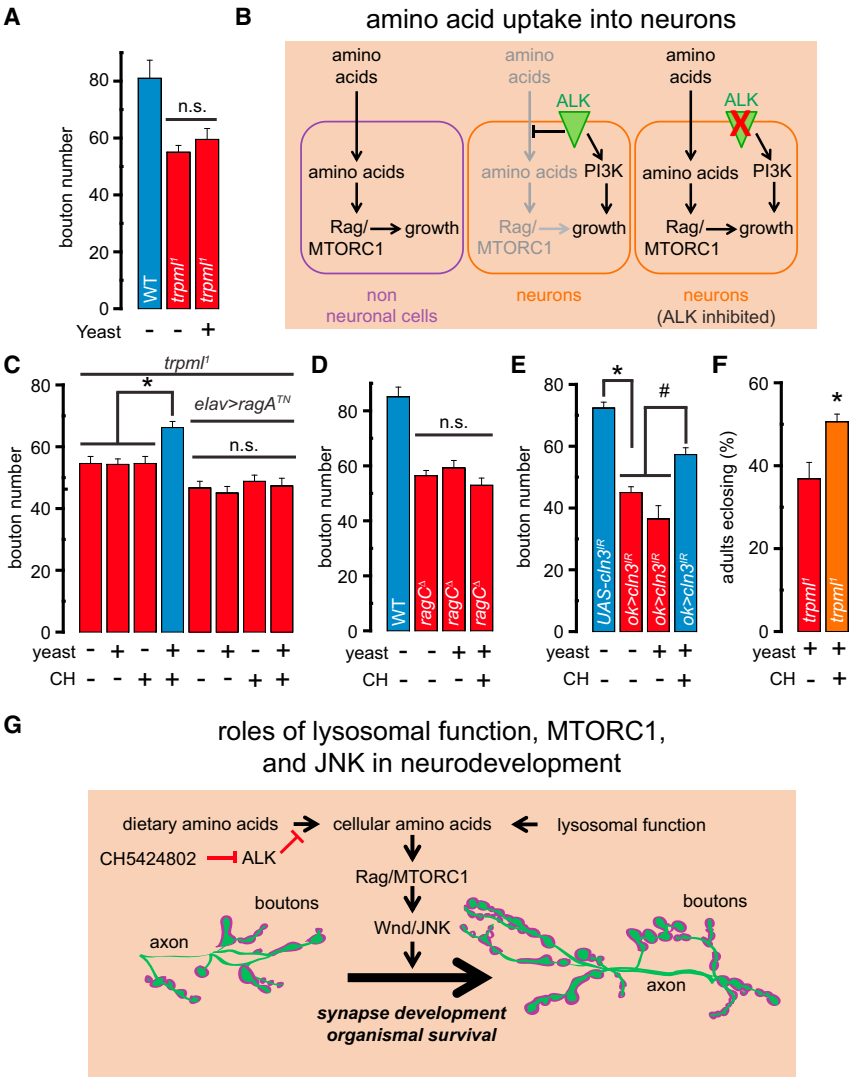

Figure 7. Simultaneous Administration of ALK inhibitor and High-Protein Diet Enhances Synaptic Growth and Adult Viability following Lysosomal Dysfunction

(A) Bar graph showing the average bouton numbers in animals of the indicated genotypes reared on instant food with the indicated additions.

(B) Mechanism of ALK-dependent block of amino acid uptake in neuronal cells.

(C–E) Bars graph showing the average bouton numbers in animals of the indicated genotypes reared on instant food with the indicated additions.

(F) Bar graph showing the percentage of the *trpml*^{1} adults that eclose from their pupal cases when reared on instant food with the indicated additions. The "+" and "−" in (C)–(F) represent presence or absence of CH5424802 or yeast. Although rearing larvae on instant food resulted in an overall increase in the number of boutons in all the genotypes, the *trpml*^{1}, *ragC*$^{\Delta}$, and *ok>cln3*^{IR} larvae showed a relative decrease in NMJ boutons, and all comparisons were made between animals reared under identical conditions.

(G) Roles of lysosomal function, MTORC1 activity, and Wnd/JNK signaling in neurodevelopment.

* and # represent statistical significance. Abbreviations: n.s., not significant; CH, CH5424802. Data shown indicate mean ± SEM.

which are critical for normal NMJ development (Figure 7G). Despite the requirement for MTORC1 in NMJ synapse development, previous studies and our current findings show that bouton numbers are independent of S6K and 4E-BP1. Rather, MTORC1 promotes NMJ growth via a MAP kinase cascade culminating in JNK activation (Figure 7G). Therefore, decreasing lysosomal function or Rag/MTORC1 activation in *hiw*^{ND8} suppressed the associated synaptic overgrowth. However, the "small-bouton" phenotype of *hiw*^{ND8} was independent of MTORC1. Thus, MTORC1 is required for JNK-dependent regulation of bouton numbers, whereas bouton morphology is independent of MTORC1. Furthermore, although both *rheb* expression and *hiw* loss result in Wnd-dependent elevation in bouton numbers, the supernumerary boutons in each case show distinct morphological features. Additional studies are needed for deciphering the complex interplay between MTORC1-JNK in regulating the NMJ morphology.

Biochemical analyses revealed that both JNK phosphorylation and its transcriptional output correlated with the activity of MTORC1, which are consistent with prior observations that *cln3* overexpression promotes JNK activation (Tuxworth et al., 2009) and that *tsc1/tsc2* deletion in flies result in increased JNK-dependent transcription (Gordon et al., 2013). These findings point to the remarkable versatility of MTORC1 in controlling both protein translation and gene transcription.

Using an in vitro kinase assay, we demonstrate that Wnd is a target of MTORC1. Because axonal injury activates both MTORC1 and DLK/JNK (Abe et al., 2010; Kenney and Kocsis, 1998; Valakh et al., 2015), our findings imply a functional connection between these two pathways. Interestingly, our data also suggest that MTORC1 contains additional kinases besides MTOR that can phosphorylate Wnd. One possibility is that ULK1/Atg1, which associates with MTORC1 (Figure S3A; Hosokawa et al., 2009), could be the kinase that phosphorylates Wnd. Consistent with this notion, overexpression of Atg1 in the *Drosophila* neurons has been shown to promote JNK signaling and NMJ synapse overgrowth via Wnd (Shen and Ganetzky, 2009).

We also found that developmental JNK activation in axonal tracts of the CC and pJNK levels in cortical neurons were compromised in a mouse model of Batten disease. Thus, the signaling deficits we identified in *Drosophila* are also conserved in mammals. The activity of DLK (the mouse homolog of Wnd) and JNK signaling are critical for axonal development in the mouse CNS (Hirai et al., 2006). Therefore, decreased neuronal JNK activation during development might underlie the thinning of the axonal tracts observed in many LSDs.

Simultaneous Administration of an ALK Inhibitor and a High-Protein Diet Rescues the Synaptic Growth Defects and Pupal Lethality Associated with Lysosomal Dysfunction

Although our findings demonstrate a role for an amino-acid-responsive cascade in the synaptic defects associated with lysosomal dysfunction, simply elevating the dietary protein content was not sufficient to rescue these defects. These findings were reminiscent of an elegant study that showed that the growth of *Drosophila* neuroblasts is uncoupled from dietary amino acids owing to the function of ALK, which suppresses the uptake of amino acids into the neuroblasts (Cheng et al., 2011b). Indeed, simultaneous administration of an ALK inhibitor and a high-protein diet partially rescued the synaptic growth defects associated with the lysosomal dysfunction, and improved the rescue of pupal lethality associated with *trpml*^{1}. Although our studies do not causally link the defects in synapse development with pupal lethality, they do raise the intriguing possibility that multiple phenotypes associated with LSDs could be targeted using ALK inhibitors along with a protein-rich diet.

Although LSDs result in lysosomal dysfunction throughout the body, neurons are exceptionally sensitive to these alterations (Bellettato and Scarpa, 2010). The cause for this sensitivity remains incompletely understood. Given our findings that mature neurons do not efficiently take up amino acids from the extracellular medium, lysosomal degradation of proteins serves as a major source of free amino acids in these cells. Therefore, disruption of lysosomal degradation leads to severe shortage of free amino acids in neurons, regardless of the quantity of dietary proteins, thus explaining the exquisite sensitivity of neurons to lysosomal dysfunction.

EXPERIMENTAL PROCEDURES

Immunohistochemistry and Immunofluorescence

Drosophila

Wandering third-instar larvae were pinned on Sylgard (Dow Corning) and bathed in ice-cold PBS. The body wall was cut along the dorsal midline, and visceral organs were removed. The fillets were pinned flat and fixed with 4% paraformaldehyde in PBS for 30 min. Fixed fillets were washed with 0.1% Triton X-100 in PBS before primary antibody incubation. Antibody dilutions were as follows: 1:200 rabbit α-horseradish peroxidase (α-HRP) (Jackson), 1:100 mouse α-DLG, 1:500 rabbit α-GFP (Invitrogen), 1:500 mouse α-myc (Sigma-Aldrich), 1:1,000 rabbit α-pMAD (Persson et al., 1998), 1:100 rabbit α-pMAD (S463/465) (41D10, Cell Signaling), 1:100 mouse α-β-gal (40-1a), and 1:500 mouse α-Wg. After incubation with primary antibodies overnight at 4°C, the fillets were washed and probed with appropriate fluorophore-conjugated secondary antibodies (Alexa Fluor 488/568/647 goat anti-mouse/rabbit/guinea pig) (Invitrogen) at room temperature for 1.5 hr. Samples were mounted on glass slide with DAPI-containing Vectashield (Vector Laboratories). The monoclonal antibodies against DLG, β-gal, and Wg were obtained from the Developmental Studies Hybridoma Bank (DSHB) developed under the auspices of the NICHD and maintained by the Department of Biology at the University of Iowa.

Mice

Brains from E19.5 mice were fixed with 10% formalin (Sigma-Aldrich) at 4°C overnight, and processed for decalcification for 2 days with Gooding and Stewart's fluid (15% formic acid, 5% formaldehyde 37%). They were then dehydrated gradually (70% to 100% ethanol), equilibrated with chloroform, embedded in paraffin blocks, and sectioned at 10 μm thickness. The sections were subjected to the immunohistochemistry using mouse monoclonal antibodies against JNK (BD, 1:200) and rabbit polyclonal antibodies against pJNK (Cell Signaling, 1:400). The Vectastain Elite ABC kit (Vector Laboratories) was used for the immunohistochemistry according to the manufacturer's protocol.

For immunofluorescence, the sections were permeabilized with 0.3% Triton X-100 in PBS and blocked for 2 hr at room temperature with 1% serum, 0.05% Triton X-100 in PBS. The slides were washed in PBS and incubated with the primary antibody for 1 day at 4°. After washing, secondary antibodies (donkey anti-rabbit Alexa Fluor 594), were added (1:200) for 2 hr. The slides were then mounted in Vectashield.

Western Blots

Drosophila

Brains or fat bodies from wandering third-instar larvae were dissected in ice-cold HL-3 (70 mM NaCl, 5 mM KCl, 20 mM $MgCl_2$, 10 mM $NaHCO_3$, 0.1 mM $CaCl_2$, 115 mM sucrose, 5 mM trehalose, and 5 mM HEPES [pH 7.2]). Six to eight brains or three to four fat bodies per genotype were triturated in 30 μl Laemmli sample buffer (Bio-Rad) with 5% 2-mercaptoethanol (Calbiochem) and heated at 96°C for 10 min. For acute CH5424802 treatment, four brains were dissected in HL-3 (containing 1 mM $CaCl_2$) with or without 1 μM CH5424802 for 1 hr before being triturated and heated in sample buffer. Total lysates were centrifuged at 10,000 × *g* for 4 min before loading the supernatant onto 4%–20% gradient gel (Bio-Rad) for SDS-PAGE. Separated proteins were transferred onto nitrocellulose blot before blocking (Odyssey Blocking Buffer, LI-COR Biosciences). The blot was probed by primary antibody mixture containing 1:5,000 rabbit α-pJNK (Promega), 1:200 rabbit α-JNK (Santa Cruz), 1:1,000 rabbit α-phospho-*Drosophila* p70 S6K (Cell Signaling), 1:1,000 rabbit α-pAKT^{S473} (Cell Signaling), or 1:1,000 mouse α-alpha-tubulin (12G10, DSHB). The secondary antibodies used were IRDye 680LT (anti-rabbit) and IRDye 800CW (anti-mouse) (LI-COR Biosciences). The bands were detected by the Odyssey imaging platform (LI-COR Biosciences). Band intensities were quantified using ImageJ.

Mice

Cerebral cortices were dissected from E17.5 mouse embryos and homogenized in ice-cold lysis buffer (20 mM Tris-HCl [pH 7.4], 150 mM NaCl, 2 mM EDTA, 1% Triton X-100, and 10% glycerol in presence of protease and phosphatase inhibitor [Roche]). Following SDS-PAGE, membranes were blocked in 5% BSA and incubated with the primary antibodies mouse monoclonal JNK (BD Biosciences, 1:500) and rabbit polyclonal pJNK (Cell Signaling, 1:1000) overnight at 4°C. Blot images were acquired using the LAS 4000 gel imaging system (GE Healthcare) and quantified using ImageJ.

In Vitro Kinase Assay

MTORC1 was preincubated (30°C, 15 min) with Torin1 (10 μM) or vehicle in kinase assay buffer (in mM: 50 KCl, 10 $MgCl_2$, 1 DTT, 25 HEPES [pH7.4]). For the radioactive kinase assay, the purified proteins (GST-Wnd^{KD}, GST-mut-Wnd^{KD}, or GST) and the kinase assay buffer containing 50 μM ATP and [γ-^{32}P] ATP (10 μCi per reaction) were added to the preincubated MTORC1 reaction mixture. Kinase reaction was performed (30°C, 30 min) and stopped by boiling in Laemmli sample buffer and resolved on SDS-PAGE gels followed by silver staining. Phosphorylated proteins were visualized by autoradiography of dried gels, and ^{32}P signals were quantified by densitometry. For the in vitro kinase assay on recombinant 4E-BP1, kinase assay buffer containing 150 ng recombinant 4E-BP1 (Santa Cruz) and 500 μM ATP was mixed with MTORC1 preincubated with Torin1 (10 μM) or vehicle. Reactions were performed at 29°C for 30 min and stopped by boiling the samples in Laemmli buffer. Samples were subsequently analyzed by SDS-PAGE and western blotting with anti-phospho-4E-BP1 (T37/46) and anti-4E-BP1 antibodies (Cell Signaling).

Statistical Analysis

Paired or unpaired Student's t tests were employed for pairwise comparisons. For comparison of three or more values, one-way ANOVA was performed to determine significance. The Bonferroni post hoc correction was applied when performing multiple pairwise comparisons. All values shown in bar graphs represent mean ± SEM. Please consult the Supplemental Experimental Procedures for all values in the bar graphs and information on statistical tests employed.

SUPPLEMENTAL INFORMATION

Supplemental Information includes Supplemental Experimental Procedures and four figures and can be found with this article online at http://dx.doi.org/10.1016/j.celrep.2015.08.047.

ACKNOWLEDGMENTS

We thank the Bloomington *Drosophila* Stock Center and Drs. H. Bellen, Y. Wairkar, G. Tear, and A. Diantonio for fly stocks and Dr. D. Sabatini for cells stably expressing FLAG-Raptor. We are grateful to N. Haelterman, K. Chen, L. Mangieri and Drs. M. Jaiswal, S. Yamamoto, and N. Giagtzoglou for scientific discussions and Dr. C.K. Yao and H. Hu for technical help. This study was supported by NIH grants R01NS081301 (K.V.), R01NS079618 (M.S.), R01NS069844 (C.A.C.), and R01DK092590 and R01AR059847 (both to R.B).

Received: April 29, 2015
Revised: July 20, 2015
Accepted: August 14, 2015
Published: September 17, 2015

REFERENCES

Abe, N., Borson, S.H., Gambello, M.J., Wang, F., and Cavalli, V. (2010). Mammalian target of rapamycin (mTOR) activation increases axonal growth capacity of injured peripheral nerves. J. Biol. Chem. *285*, 28034–28043.

Autti, T., Raininko, R., Vanhanen, S.L., and Santavuori, P. (1996). MRI of neuronal ceroid lipofuscinosis. I. Cranial MRI of 30 patients with juvenile neuronal ceroid lipofuscinosis. Neuroradiology *38*, 476–482.

Ballard, S.L., Miller, D.L., and Ganetzky, B. (2014). Retrograde neurotrophin signaling through Tollo regulates synaptic growth in Drosophila. J. Cell Biol. *204*, 1157–1172.

Bar-Peled, L., Schweitzer, L.D., Zoncu, R., and Sabatini, D.M. (2012). Ragulator is a GEF for the rag GTPases that signal amino acid levels to mTORC1. Cell *150*, 1196–1208.

Bargal, R., Avidan, N., Ben-Asher, E., Olender, Z., Zeigler, M., Frumkin, A., Raas-Rothschild, A., Glusman, G., Lancet, D., and Bach, G. (2000). Identification of the gene causing mucolipidosis type IV. Nat. Genet. *26*, 118–123.

Bassi, M.T., Manzoni, M., Monti, E., Pizzo, M.T., Ballabio, A., and Borsani, G. (2000). Cloning of the gene encoding a novel integral membrane protein, mucolipidin-and identification of the two major founder mutations causing mucolipidosis type IV. Am. J. Hum. Genet. *67*, 1110–1120.

Bellettato, C.M., and Scarpa, M. (2010). Pathophysiology of neuropathic lysosomal storage disorders. J. Inherit. Metab. Dis. *33*, 347–362.

Cheng, L., Locke, C., and Davis, G.W. (2011a). S6 kinase localizes to the presynaptic active zone and functions with PDK1 to control synapse development. J. Cell Biol. *194*, 921–935.

Cheng, L.Y., Bailey, A.P., Leevers, S.J., Ragan, T.J., Driscoll, P.C., and Gould, A.P. (2011b). Anaplastic lymphoma kinase spares organ growth during nutrient restriction in Drosophila. Cell *146*, 435–447.

Collins, C.A., and DiAntonio, A. (2007). Synaptic development: insights from Drosophila. Curr. Opin. Neurobiol. *17*, 35–42.

Collins, C.A., Wairkar, Y.P., Johnson, S.L., and DiAntonio, A. (2006). Highwire restrains synaptic growth by attenuating a MAP kinase signal. Neuron *51*, 57–69.

Cotman, S.L., Vrbanac, V., Lebel, L.A., Lee, R.L., Johnson, K.A., Donahue, L.R., Teed, A.M., Antonellis, K., Bronson, R.T., Lerner, T.J., and MacDonald, M.E. (2002). Cln3(Deltaex7/8) knock-in mice with the common JNCL mutation exhibit progressive neurologic disease that begins before birth. Hum. Mol. Genet. *11*, 2709–2721.

Curcio-Morelli, C., Charles, F.A., Micsenyi, M.C., Cao, Y., Venugopal, B., Browning, M.F., Dobrenis, K., Cotman, S.L., Walkley, S.U., and Slaugenhaupt, S.A. (2010). Macroautophagy is defective in mucolipin-1-deficient mouse neurons. Neurobiol. Dis. *40*, 370–377.

DiAntonio, A., Haghighi, A.P., Portman, S.L., Lee, J.D., Amaranto, A.M., and Goodman, C.S. (2001). Ubiquitination-dependent mechanisms regulate synaptic growth and function. Nature *412*, 449–452.

Dong, X.P., Shen, D., Wang, X., Dawson, T., Li, X., Zhang, Q., Cheng, X., Zhang, Y., Weisman, L.S., Delling, M., and Xu, H. (2010). PI(3,5)P(2) controls membrane trafficking by direct activation of mucolipin Ca(2+) release channels in the endolysosome. Nat. Commun. *1*, 38.

Eto, K., Kawauchi, T., Osawa, M., Tabata, H., and Nakajima, K. (2010). Role of dual leucine zipper-bearing kinase (DLK/MUK/ZPK) in axonal growth. Neurosci. Res. *66*, 37–45.

Feng, X., Huang, Y., Lu, Y., Xiong, J., Wong, C.O., Yang, P., Xia, J., Chen, D., Du, G., Venkatachalam, K., et al. (2014a). Drosophila TRPML forms PI(3,5)P2-activated cation channels in both endolysosomes and plasma membrane. J. Biol. Chem. *289*, 4262–4272.

Feng, X., Xiong, J., Lu, Y., Xia, X., and Zhu, M.X. (2014b). Differential mechanisms of action of the mucolipin synthetic agonist, ML-SA1, on insect TRPML and mammalian TRPML1. Cell Calcium *56*, 446–456.

Frei, K.P., Patronas, N.J., Crutchfield, K.E., Altarescu, G., and Schiffmann, R. (1998). Mucolipidosis type IV: characteristic MRI findings. Neurology *51*, 565–569.

Geuking, P., Narasimamurthy, R., Lemaitre, B., Basler, K., and Leulier, F. (2009). A non-redundant role for Drosophila Mkk4 and hemipterous/Mkk7 in TAK1-mediated activation of JNK. PLoS ONE *4*, e7709.

Gordon, G.M., Zhang, T., Zhao, J., and Du, W. (2013). Deregulated G1-S control and energy stress contribute to the synthetic-lethal interactions between inactivation of RB and TSC1 or TSC2. J. Cell Sci. *126*, 2004–2013.

Hara, K., Maruki, Y., Long, X., Yoshino, K., Oshiro, N., Hidayat, S., Tokunaga, C., Avruch, J., and Yonezawa, K. (2002). Raptor, a binding partner of target of rapamycin (TOR), mediates TOR action. Cell *110*, 177–189.

Hirai, S., Cui, F., Miyata, T., Ogawa, M., Kiyonari, H., Suda, Y., Aizawa, S., Banba, Y., and Ohno, S. (2006). The c-Jun N-terminal kinase activator dual leucine zipper kinase regulates axon growth and neuronal migration in the developing cerebral cortex. J. Neurosci. *26*, 11992–12002.

Hosokawa, N., Hara, T., Kaizuka, T., Kishi, C., Takamura, A., Miura, Y., Iemura, S., Natsume, T., Takehana, K., Yamada, N., et al. (2009). Nutrient-dependent mTORC1 association with the ULK1-Atg13-FIP200 complex required for autophagy. Mol. Biol. Cell *20*, 1981–1991.

Hsu, P.P., Kang, S.A., Rameseder, J., Zhang, Y., Ottina, K.A., Lim, D., Peterson, T.R., Choi, Y., Gray, N.S., Yaffe, M.B., et al. (2011). The mTOR-regulated phosphoproteome reveals a mechanism of mTORC1-mediated inhibition of growth factor signaling. Science *332*, 1317–1322.

Jennings, J.J., Jr., Zhu, J.H., Rbaibi, Y., Luo, X., Chu, C.T., and Kiselyov, K. (2006). Mitochondrial aberrations in mucolipidosis Type IV. J. Biol. Chem. *281*, 39041–39050.

Kang, S.A., Pacold, M.E., Cervantes, C.L., Lim, D., Lou, H.J., Ottina, K., Gray, N.S., Turk, B.E., Yaffe, M.B., and Sabatini, D.M. (2013). mTORC1 phosphorylation sites encode their sensitivity to starvation and rapamycin. Science *341*, 1236566.

Kenney, A.M., and Kocsis, J.D. (1998). Peripheral axotomy induces long-term c-Jun amino-terminal kinase-1 activation and activator protein-1 binding activity by c-Jun and junD in adult rat dorsal root ganglia In vivo. J. Neurosci. *18*, 1318–1328.

Kim, E., Goraksha-Hicks, P., Li, L., Neufeld, T.P., and Guan, K.L. (2008). Regulation of TORC1 by Rag GTPases in nutrient response. Nat. Cell Biol. *10*, 935–945.

Knox, S., Ge, H., Dimitroff, B.D., Ren, Y., Howe, K.A., Arsham, A.M., Easterday, M.C., Neufeld, T.P., O'Connor, M.B., and Selleck, S.B. (2007). Mechanisms of TSC-mediated control of synapse assembly and axon guidance. PLoS ONE *2*, e375.

Kristensen, K., and Lou, H.C. (1983). Central nervous system dysfunction as early sign of neuronal ceroid lipofuscinosis (Batten's disease). Dev. Med. Child Neurol. *25*, 588–590.

Lee, S., Liu, H.P., Lin, W.Y., Guo, H., and Lu, B. (2010). LRRK2 kinase regulates synaptic morphology through distinct substrates at the presynaptic and postsynaptic compartments of the Drosophila neuromuscular junction. J. Neurosci. *30*, 16959–16969.

Marqués, G., Bao, H., Haerry, T.E., Shimell, M.J., Duchek, P., Zhang, B., and O'Connor, M.B. (2002). The Drosophila BMP type II receptor Wishful Thinking regulates neuromuscular synapse morphology and function. Neuron *33*, 529–543.

Martín-Blanco, E., Gampel, A., Ring, J., Virdee, K., Kirov, N., Tolkovsky, A.M., and Martinez-Arias, A. (1998). puckered encodes a phosphatase that mediates a feedback loop regulating JNK activity during dorsal closure in Drosophila. Genes Dev. *12*, 557–570.

Miech, C., Pauer, H.U., He, X., and Schwarz, T.L. (2008). Presynaptic local signaling by a canonical wingless pathway regulates development of the Drosophila neuromuscular junction. J. Neurosci. *28*, 10875–10884.

Miedel, M.T., Rbaibi, Y., Guerriero, C.J., Colletti, G., Weixel, K.M., Weisz, O.A., and Kiselyov, K. (2008). Membrane traffic and turnover in TRP-ML1-deficient cells: a revised model for mucolipidosis type IV pathogenesis. J. Exp. Med. *205*, 1477–1490.

Mitchison, H.M., Taschner, P.E., Kremmidiotis, G., Callen, D.F., Doggett, N.A., Lerner, T.J., Janes, R.B., Wallace, B.A., Munroe, P.B., O'Rawe, A.M., et al. (1997). Structure of the CLN3 gene and predicted structure, location and function of CLN3 protein. Neuropediatrics *28*, 12–14.

Munroe, P.B., Mitchison, H.M., O'Rawe, A.M., Anderson, J.W., Boustany, R.M., Lerner, T.J., Taschner, P.E., de Vos, N., Breuning, M.H., Gardiner, R.M., and Mole, S.E. (1997). Spectrum of mutations in the Batten disease gene, CLN3. Am. J. Hum. Genet. *61*, 310–316.

Natarajan, R., Trivedi-Vyas, D., and Wairkar, Y.P. (2013). Tuberous sclerosis complex regulates Drosophila neuromuscular junction growth via the TORC2/Akt pathway. Hum. Mol. Genet. *22*, 2010–2023.

Packard, M., Koo, E.S., Gorczyca, M., Sharpe, J., Cumberledge, S., and Budnik, V. (2002). The Drosophila Wnt, wingless, provides an essential signal for pre- and postsynaptic differentiation. Cell *111*, 319–330.

Pennetta, G., Hiesinger, P.R., Fabian-Fine, R., Meinertzhagen, I.A., and Bellen, H.J. (2002). Drosophila VAP-33A directs bouton formation at neuromuscular junctions in a dosage-dependent manner. Neuron *35*, 291–306.

Persson, U., Izumi, H., Souchelnytskyi, S., Itoh, S., Grimsby, S., Engström, U., Heldin, C.H., Funa, K., and ten Dijke, P. (1998). The L45 loop in type I receptors for TGF-beta family members is a critical determinant in specifying Smad isoform activation. FEBS Lett. *434*, 83–87.

Rämet, M., Lanot, R., Zachary, D., and Manfruelli, P. (2002). JNK signaling pathway is required for efficient wound healing in Drosophila. Dev. Biol. *241*, 145–156.

Riesgo-Escovar, J.R., Jenni, M., Fritz, A., and Hafen, E. (1996). The Drosophila Jun-N-terminal kinase is required for cell morphogenesis but not for DJun-dependent cell fate specification in the eye. Genes Dev. *10*, 2759–2768.

Rohrbough, J., Kent, K.S., Broadie, K., and Weiss, J.B. (2013). Jelly Belly trans-synaptic signaling to anaplastic lymphoma kinase regulates neurotransmission strength and synapse architecture. Dev. Neurobiol. *73*, 189–208.

Roos, J., Hummel, T., Ng, N., Klämbt, C., and Davis, G.W. (2000). Drosophila Futsch regulates synaptic microtubule organization and is necessary for synaptic growth. Neuron *26*, 371–382.

Sakamoto, H., Tsukaguchi, T., Hiroshima, S., Kodama, T., Kobayashi, T., Fukami, T.A., Oikawa, N., Tsukuda, T., Ishii, N., and Aoki, Y. (2011). CH5424802, a selective ALK inhibitor capable of blocking the resistant gatekeeper mutant. Cancer Cell *19*, 679–690.

Sancak, Y., Peterson, T.R., Shaul, Y.D., Lindquist, R.A., Thoreen, C.C., Bar-Peled, L., and Sabatini, D.M. (2008). The Rag GTPases bind raptor and mediate amino acid signaling to mTORC1. Science *320*, 1496–1501.

Sanyal, S., Sandstrom, D.J., Hoeffer, C.A., and Ramaswami, M. (2002). AP-1 functions upstream of CREB to control synaptic plasticity in Drosophila. Nature *416*, 870–874.

Shen, W., and Ganetzky, B. (2009). Autophagy promotes synapse development in Drosophila. J. Cell Biol. *187*, 71–79.

Shen, D., Wang, X., Li, X., Zhang, X., Yao, Z., Dibble, S., Dong, X.P., Yu, T., Lieberman, A.P., Showalter, H.D., and Xu, H. (2012). Lipid storage disorders block lysosomal trafficking by inhibiting a TRP channel and lysosomal calcium release. Nat. Commun. *3*, 731.

Slupianek, A., Nieborowska-Skorska, M., Hoser, G., Morrione, A., Majewski, M., Xue, L., Morris, S.W., Wasik, M.A., and Skorski, T. (2001). Role of phosphatidylinositol 3-kinase-Akt pathway in nucleophosmin/anaplastic lymphoma kinase-mediated lymphomagenesis. Cancer Res. *61*, 2194–2199.

Stewart, R., Akhmedov, D., Robb, C., Leiter, C., and Berdeaux, R. (2013). Regulation of SIK1 abundance and stability is critical for myogenesis. Proc. Natl. Acad. Sci. USA *110*, 117–122.

Stocker, H., Radimerski, T., Schindelholz, B., Wittwer, F., Belawat, P., Daram, P., Breuer, S., Thomas, G., and Hafen, E. (2003). Rheb is an essential regulator of S6K in controlling cell growth in Drosophila. Nat. Cell Biol. *5*, 559–565.

Sun, M., Goldin, E., Stahl, S., Falardeau, J.L., Kennedy, J.C., Acierno, J.S., Jr., Bove, C., Kaneski, C.R., Nagle, J., Bromley, M.C., et al. (2000). Mucolipidosis type IV is caused by mutations in a gene encoding a novel transient receptor potential channel. Hum. Mol. Genet. *9*, 2471–2478.

Sweeney, S.T., and Davis, G.W. (2002). Unrestricted synaptic growth in *spinster*-a late endosomal protein implicated in TGF-β-mediated synaptic growth regulation. Neuron *36*, 403–416.

Thoreen, C.C., Kang, S.A., Chang, J.W., Liu, Q., Zhang, J., Gao, Y., Reichling, L.J., Sim, T., Sabatini, D.M., and Gray, N.S. (2009). An ATP-competitive mammalian target of rapamycin inhibitor reveals rapamycin-resistant functions of mTORC1. J. Biol. Chem. *284*, 8023–8032.

Tuxworth, R.I., Vivancos, V., O'Hare, M.B., and Tear, G. (2009). Interactions between the juvenile Batten disease gene, CLN3, and the Notch and JNK signalling pathways. Hum. Mol. Genet. *18*, 667–678.

Valakh, V., Frey, E., Babetto, E., Walker, L.J., and DiAntonio, A. (2015). Cytoskeletal disruption activates the DLK/JNK pathway, which promotes axonal regeneration and mimics a preconditioning injury. Neurobiol. Dis. *77*, 13–25.

Vellodi, A. (2005). Lysosomal storage disorders. Br. J. Haematol. *128*, 413–431.

Venkatachalam, K., Long, A.A., Elsaesser, R., Nikolaeva, D., Broadie, K., and Montell, C. (2008). Motor deficit in a *Drosophila* model of mucolipidosis type IV due to defective clearance of apoptotic cells. Cell *135*, 838–851.

Venkatachalam, K., Wong, C.O., and Montell, C. (2013). Feast or famine: role of TRPML in preventing cellular amino acid starvation. Autophagy *9*, 98–100.

Venkatachalam, K., Wong, C.O., and Zhu, M.X. (2015). The role of TRPMLs in endolysosomal trafficking and function. Cell Calcium *58*, 48–56.

Vergarajauregui, S., and Puertollano, R. (2008). Mucolipidosis type IV: the importance of functional lysosomes for efficient autophagy. Autophagy *4*, 832–834.

Wan, H.I., DiAntonio, A., Fetter, R.D., Bergstrom, K., Strauss, R., and Goodman, C.S. (2000). Highwire regulates synaptic growth in Drosophila. Neuron *26*, 313–329.

Wong, C.O., Li, R., Montell, C., and Venkatachalam, K. (2012). Drosophila TRPML is required for TORC1 activation. Curr. Biol. *22*, 1616–1621.

Wong, C.O., Chen, K., Lin, Y.Q., Chao, Y., Duraine, L., Lu, Z., Yoon, W.H., Sullivan, J.M., Broadhead, G.T., Sumner, C.J., et al. (2014). A TRPV channel in Drosophila motor neurons regulates presynaptic resting Ca2+ levels, synapse growth, and synaptic transmission. Neuron *84*, 764–777.

Yip, C.K., Murata, K., Walz, T., Sabatini, D.M., and Kang, S.A. (2010). Structure of the human mTOR complex I and its implications for rapamycin inhibition. Mol. Cell *38*, 768–774.

Zhang, C.S., Jiang, B., Li, M., Zhu, M., Peng, Y., Zhang, Y.L., Wu, Y.Q., Li, T.Y., Liang, Y., Lu, Z., et al. (2014). The lysosomal v-ATPase-Ragulator complex is a common activator for AMPK and mTORC1, acting as a switch between catabolism and anabolism. Cell Metab. *20*, 526–540.

Zoncu, R., Efeyan, A., and Sabatini, D.M. (2011). mTOR: from growth signal integration to cancer, diabetes and ageing. Nat. Rev. Mol. Cell Biol. *12*, 21–35.

Cell Reports

Supplemental Information

Diminished MTORC1-Dependent JNK Activation Underlies Neurodevelopmental Defects Associated with Lysosomal Dysfunction

Ching-On Wong, Michela Palmieri, Jiaxing Li, Dmitry Akhmedov, Yufang Chao, Geoffrey T. Broadhead, Michael X. Zhu, Rebecca Berdeaux, Catherine A. Collins, Marco Sardiello, and Kartik Venkatachalam

Inventory of Supplemental Materials

Diminished MTORC1-Dependent JNK-Activation Underlies the Neurodevelopmental Defects Associated with Lysosomal Dysfunction

Ching-On Wong, Michela Palmieri, Jiaxing Li, Dmitry Akhmedov, Yufang Chao, Geoffrey T. Broadhead, Michael X. Zhu, Rebecca Berdeaux, Catherine A. Collins, Marco Sardiello, and Kartik Venkatachalam

SUPPLEMENTAL MATERIALS

Supplemental Experimental Procedures

Drosophila strains

The wild-type *Drosophila* strains used in the study were *Canton S* and w^{1118}. The *trpml* related strains used were: $trpml^{1}$, $trpml^{2}$, *UAS-trpml*, P[$trpml^{+}$], and Df^{trpml} (*Df(3L)Exel6135*) (all from (Venkatachalam et al., 2008)) and *UAS-trpml::myc* (Wong et al., 2012). Other *Drosophila* strains used in this study were *UAS-spinster::gfp* (Sweeney and Davis, 2002), *UAS-lamp::gfp* (Pulipparacharuvil et al., 2005), *elav-GAL4* (Lin and Goodman, 1994), *C164-GAL4* (Brand and Perrimon, 1993), *mef2-GAL4* (Ranganayakulu et al., 1996), *cg-GAL4* (Hennig et al., 2006), $ragC^{\Delta}$ (Kim et al., 2008), *UAS-*$ragA^{TN}$ (Kim et al., 2008), *UAS-*$ragA^{QL}$ (Kim et al., 2008), *n-syb-GAL4* (Pauli et al., 2008), P{*TRiP.JF01088*} (*UAS-*$raptor^{IR}$) (Bloomington *Drosophila* Stock Center) (Kockel et al., 2010; Lee and Chung, 2007; Natarajan et al., 2013), *vglut*^{ok371}*-GAL4* (*ok371-GAL4*) (Brand and Perrimon, 1993; Meyer and Aberle, 2006), *UAS-*$S6K^{KQ}$ (Barcelo and Stewart, 2002), *UAS-thor* (Bloomington *Drosophila* Stock Center), bsk^{1} (Sluss et al., 1996), wnd^{3} (Collins et al., 2006), *UAS-hiw* (Wu et al., 2005), hiw^{ND8} (Wan et al., 2000), *UAS-rheb* (Stocker et al., 2003), *puc-LacZ* (Martin-Blanco et al., 1998), *BG380-GAL4* (Budnik, 1996), and P{*TRiP.HMS01476*} (*UAS-*$cln3^{IR}$) (Bloomington *Drosophila* Stock Center).

Fly husbandry and chemical feeding

All flies were reared at room temperature (~22°C). Except for the experiments with ML-SA1, yeast, or CH5424802 feeding, all flies were raised in standard fly food (1 L of food contained: 95 g agar, 275 g Brewer's yeast, 520 g of cornmeal, 110 g of sugar, 45 g of

propionic acid, and 36 g of Tegosept). For the drug-feeding experiments, the food was comprised of 1.25 g of instant fly food (formula 4-24 plain, Carolina Biological Supply Company) with 0.125 g of inactive yeast suspended in 3 mL water. For chloroquine feeding experiments, 2 mM chloroquine was added to the food. For ML-SA1 feeding experiments, 20 μM ML-SA1 or 0.1% DMSO was added to the food suspension. For CH5424802 feeding experiments, 1 μM CH5424802 or 0.02% DMSO in 0.5 mL water was added to the fly food on day 5 after egg deposition. Subsequently, an additional 0.5 mL water or 0.5 mL yeast paste (40% w/v) containing CH5424802 (1 μM) or DMSO (0.02%) was laid on top of the fly food.

Image acquisition and quantification

Confocal images of *Drosophila* samples were acquired using a Nikon A1 Confocal Laser Microscope System (Nikon) as Z-series at 1 μm steps. For NMJ bouton number quantification, a 60x oil-immersion objective was used to focus on the NMJ (muscle 6/7, A3 segment). Only type 1 boutons with both HRP- and DLG-positive signals were counted. To isolate the pMAD and Wg signals within the NMJ, masks were applied to eliminate the pMAD and Wg signal outside the DLG-positive regions using Image Pro Plus (Media Cybernetics). Eps15 staining was used in these experiments as a control for antibody staining.

For analysis of expression from *puc*-lacZ reporter, images of larval VNCs were obtained on an Improvision spinning disk confocal microscope (Perkin Elmer), using a 40x oil-immersion objective and 0.8 μm steps. The MN cell bodies along the dorsal midline of the nerve cord in segments A2-A5 were identified based on P-Smad1/5

staining, and Volocity software (Perkin Elmer) was used to measure the mean intensities of β-gal staining in these nuclei. The mean intensity in these MNs per animal was measured for at least 4 animals per genotype, and normalized to *puc-lacZ* expression in controls that were processed in parallel for immunocytochemistry and imaging.

Immunohistochemical images of mouse brain tissues were acquired on a Leica DM RXA2 microscope with Hitachi HVC20A camera, and confocal images of mouse brain tissues were acquired on a Zeiss LSM 710 microscope.

Protein purification

Drosophila Wnd cDNA was sub-cloned into pGEX-KG expression vector. The codon encoding lysine^{188} was mutated to encode an alanine (K188A) to yield GST-tagged Wnd^{KD}. To mutate the putative MTORC1 target sites on Wnd^{KD}, the codons encoding serine^{305}, threonine^{309}, serine^{362}, and serine^{392} were all mutated to encode alanines. The resulting construct was named mut-Wnd^{KD}. The expression constructs were then transformed into BL21-CodonPlus competent *E. coli* cells (Stratagene). IPTG was added to the *E. coli* culture to induce protein expression at 30°C. Total protein was harvested by sonication. The recombinant GST-tagged proteins were purified using glutathione sepharose (GE Life Sciences).

The MTORC1 complex was purified from HEK293T cells stably expressing FLAG-tagged Raptor (FLAG-Raptor) using anti-FLAG M2 Agarose (Sigma-Aldrich). The procedures were followed as described (Yip et al., 2010), except the gel filtration step. The input, flow-through, wash, and eluate fractions were analyzed by SDS-PAGE and

Western blot with anti-MTOR (Cell Signaling), anti-FLAG (Cell Signaling), anti-ULK1 (Cell Signaling), anti-JNK (Santa Cruz), and anti-α-tubulin (DSHB). Eluate fraction 2 (Figure S3) was used for the *in vitro* kinase assay.

Statistical Analysis

Figure 1H Number of boutons: WT (w^{1118}) = 66.7±2.1, $trpml^{1}$ = 46.0±2.3, $trpml^{2}$ = 48.3±3.6, $trpml^{1}/trpml^{2}$ = 43.8±2.6, $trpml^{1}/Df^{trpml}$= 42.7±2.9, P[$trpml^{+}$]; $trpml^{1}$ = 64.5±3.5; *, p = $6.3x10^{-14}$, ANOVA; n = 10-30 NMJs per genotype. *UAS-trpml; trpml*^{1} = 49.3±2.1, *elav-GAL4;; trpml*^{1} = 54.6±2.1, *elav>trpml; trpml*^{1} = 72.5±3.1, *C164-GAL4; trpml*^{1} = 53.7±2.1, *C164>trpml; trpml*^{1} = 71.0±2.5, *mef2-GAL4; trpml*^{1} = 50.9±3.4, *mef2>trpml; trpml*^{1} = 50.1±3.5; *, p = $6.3x10^{-14}$, ANOVA; n = 10-34 NMJs per genotype.

Figure 2H Number of boutons: $ragC^{\Delta}$/+ = 78.3±2.9, $ragC^{\Delta}$ = 48.7±2.2, *UAS-ragA*^{TN} = 69.2±2.0, *elav-GAL4* = 83.0±8.8, *elav>ragA*^{TN} = 53.2±4.0, *UAS-ragA*^{TN}*; trpml*^{1} = 53.9±1.5, *elav-GAL4;; trpml*^{1} = 54.6±2.1, *elav>ragA*^{TN}*; trpml*^{1} = 51.8±3.3, *UAS-ragA*^{QL}*; trpml*^{1} = 46.5±1.2, *n-syb-GAL4; trpml*^{1} = 49.2±1.7, *n-syb>ragA*^{QL}*; trpml*^{1} = 69.6±3.2, *elav>ragA*^{QL}*; trpml*^{1} = 69.9±3.2, *elav>ragA*^{QL} = 73.5±5.4; *, p = $2.8x10^{-13}$, ANOVA; #, p = $1.2x10^{-4}$, ANOVA; ¶, p = $2.8x10^{-13}$, ANOVA; n = 5-30 NMJs per genotype.

Figure 2I Number of boutons: *ok371-GAL4* = 69.5±4.7, *UAS-raptor*^{IR} = 66.7±2.1, *ok371>raptor*^{IR} = 54.8±3.2, *elav-GAL4* = 83.0±8.8, *elav>raptor*^{IR} = 47.4±2.5; *, p = 0.01, ANOVA; #, p = $6.3x10^{-7}$, ANOVA; n = 8-21 NMJs per genotype.

Figure 2J % *trpml*^{1} adults eclosing: *UAS-ragA*^{QL}*; trpml*^{1} = 21.6±10.0, *elav>ragA*^{QL}*; trpml*^{1} = 81.6±13.6; *, p = 0.006, Student's t-test; n = 5-6 vials per genotype.

Figure 3G Number of boutons: *bsk*^{1}/+ = 80.2±4.7, *trpml*^{1}/+ = 70.3±2.8, *bsk*^{1}/+; *trpml*^{1}/+ = 46.7±3.1, *ragC*$^{\Delta}$ /+ = 78.3±2.9, *bsk*^{1}/ *ragC*$^{\Delta}$ = 43.8±2.9; *, p = 3.2x10^{-7}, ANOVA; #, p = 1.9x10^{-9}, ANOVA; n = 9-20 NMJs per genotype.

Figure 3H Number of boutons: *wnd*^{3}/+ = 68.6±2.7, *trpml*^{1}/+ = 70.3±2.8, *wnd*^{3}/*trpml*^{1} = 47.6±1.1; *, p = 5.9x10-10, ANOVA; n = 10-15 NMJs per genotype.

Figure 3J Number of boutons: ML-SA1 (-): *elav>hiw* = 63±2.8, elav>*hiw; trpml*^{1}/+ = 51.3±2.8, *trpml*^{1} = 50.1±1.6, ML-SA1 (+): *elav>hiw; trpml*^{1}/+ = 66.5±3.7, *trpml*^{1} = 50.2±2.8; *, p = 0.006 and #, p = 0.003, unpaired Student's t-tests; n = 7-18 NMJs per genotype.

Figure 4E Number of boutons: *hiw*^{ND8} = 108.9±3.4, *hiw*^{ND8};; *trpml*^{1} = 70.2±3.6, *hiw*^{ND8}; *UAS-ragA*^{TN} = 100.6±3.9, *hiw*^{ND8}; *ok371-GAL4* = 113.7±5.0, *hiw*^{ND8}; *ok371>ragA*^{TN} = 83.7±4.7, *hiw*^{ND8}; *UAS-raptor*^{IR} = 120±5.2, *hiw*^{ND8}; *ok371>raptor*^{IR} = 100.8±5.6; *, p = 5.1x10^{-10}, unpaired Student's t-test; #, p = 0.001, ANOVA; ¶, p = 0.02, unpaired Student's t-test; n = 6-28 NMJs per genotype.

Figure 4J Number of boutons: *UAS-rheb* = 54.8±3.3, *elav>rheb* = 121.8±9.9, *UAS-rheb, wnd*^{3}/+ = 59.2±2.4, *elav-GAL4; wnd*^{3}/+ = 67.1±4.0, *elav>rheb; wnd*^{3}/+ = 80.4±4.8; *, p = 1.9x10^{-6}, unpaired Student's t-test; #, p = 2.7x10^{-4}, unpaired Student's t-test; n = 8-18 NMJs per genotype.

Figure 5B Relative pJNK intensities (normalized to WT values): *ragC*$^{\Delta}$ = 0.64±0.08, *hiw*^{ND8} = 1.5±0.2, *hiw*^{ND8}*;; trpml*^{1} = 1.2±0.1; *, p = 0.001, unpaired Student's t-test; ¶, p = 0.01; #, p = 0.04, unpaired Student's t-tests, n = 5-7 separate samples per genotype.

Figure 5C Relative JNK intensities: *ragC*$^{\Delta}$ *normalized to* WT = 0.95±0.03, *hiw*^{ND8}*;; trpml*^{1} normalized to *hiw*^{ND8} = 1.15±0.19; n = 4-6 separate samples per genotype.

Figure 5D Relative pJNK/JNK intensities: *elav>rheb* normalized to *UAS-rheb* = 1.24±0.06; *, p = 0.005, paired Student's t-test; n = 8 samples per genotype.

Figure 5F Relative β-Gal intensities (normalized to *BG380-GAL4/+* mean): *BG380-GAL4/+* = 1±0.05, *BG380>ragA*^{TN} = 0.8±0.02, *BG380>raptor*^{IR} =0.8±0.01; *, p = 0.009, ANOVA; n = 3-4 animals per genotype.

Figure 5G Relative β-GAL intensities (normalized to *BG380-GAL4/+* mean): *BG380-GAL4/+* = 1±0.02, *BG380>rheb* = 2.6±0.5; *, p<0.003, Student's t-test; n = 7 animals per genotype.

Figure 5I Relative Wnd phosphorylation (normalized to control): GST-Wnd^{KD}: 10 μM Torin1 = 0.7±0.06; *, p = 0.0013, paired Student's t-test, n = 8; GST-mut-Wnd^{KD}: 10 μM Torin1 = 1±0.3, n = 3.

Figure 6C Number of boutons: *cln3*$^{\Delta MB1}$*/+* = 65.3±2.4, *cln3*$^{\Delta MB1}$ = 44.8±1.8, *UAS-cln3*^{IR} = 76.1±2.9, *ok371-GAL4* = 69.5±4.7, *ok371>cln3*^{IR} = 48.1±2.5; *, p = 1.5x10^{-5}, Student's t-test; #, p = 2.1x10^{-7}, ANOVA; n = 7-17 NMJs per genotype.

Figure 6D Number of boutons: *cln3*$^{\Delta MB1}$*/+* = 65.3±2.4, *trpml*^{1}*/+* = 70.3±2.8, *cln3*$^{\Delta MB1}$*/trpml*^{1} = 44.5±2.1, *UAS-ragA*^{QL}*;cln3*$^{\Delta MB1}$ = 41.2±2.2, *elav>ragA*^{QL}*;cln3*$^{\Delta MB1}$ =

69.0±4.0, *elav>ragA*^{QL} = 73.5±5.4; *, p = 1.5x10^{-8}, ANOVA; #, p = 2.7x10^{-5}, Student's t-test; n = 7-15 NMJs per genotype.

Figure 6F Relative pJNK intensities: *n-syb>cln3*^{IR} normalized to *UAS-cln3*^{IR} = 0.67±0.002; *, p = 3x10^{-5}, paired Student's t-tests, n = 3 separate samples per genotype.

Figure 6N Relative pJNK/GAPDH intensities (normalized to WT mean): WT = 1±0.02, *Cln3*$^{-/-}$ = 0.46±0.03; *, p = 0.002, paired Student's t-tests, n = 3 separate samples per genotype.

Figure 6O Relative pJNK/JNK intensities (normalized to WT mean): WT = 1±0.05, *Cln3*$^{-/-}$ = 0.57±0.02; *, p = 0.01, Student's t-tests, n = 3 separate samples per genotype.

Figure 7A Number of boutons: Yeast (-): WT = 81.0±6.4, *trpml*^{1} = 55.0±2.4; Yeast (+): *trpml*^{1} = 59.5±3.9; n = 11-14 NMJs per genotype.

Figure 7C-D Number of boutons: Yeast (-) & CH5424802 (-): *trpml*^{1} = 54.9±2.3, *elav>ragA*^{TN};*trpml*^{1} = 46.6±2.2, WT =85.1±3.5 ,*ragC* ˙ = 56.4±1.9; Yeast (+) & CH5424802 (-): *trpml*^{1} = 54.3±1.8, *elav>ragA*^{TN};*trpml*^{1} = 45±2.1, *ragC* ˙ = 59.2±2.7; Yeast (-) & CH5424802 (+): *trpml*^{1} = 51.8±2.9, *elav>ragA*^{TN};*trpml*^{1} = 48.8±2; Yeast (+) & CH5424802 (+): *trpml*^{1} = 66.2±2.0, *elav>ragA*^{TN};*trpml*^{1} = 47.3±2.5, *ragC* ˙ = 52.9±2.6; *, p = 1.1x10^{-5}, ANOVA; n = 20-32 NMJs per genotype.

Figure 7E Number of boutons in *UAS-cln3*^{IR}: Yeast (-) & CH5424802 (-) = 72.4±1.9; Number of boutons in *ok>cln3*^{IR}: Yeast (-) & CH5424802 (-) = 45.0±1.9; Yeast (+) & CH5424802 (-) = 36.5±4.3; Yeast (+) & CH5424802 (+) = 57.3±2.2; *, p = 6.6x10^{-12}, unpaired Student's t-test; #, p = 7x10^{-5}, ANOVA; n = 14-19 NMJs per genotype.

Figure 7F % adults eclosing: Yeast (+) & CH5424802 (-) = 46.1±4.9; Yeast (+) & CH5424802 (+) = 63.2±2.3; *, p = 0.03, unpaired Student's t-test; n = 4 vials per treatment.

Figure S1C Number of boutons: WT = 66.7±2.1, *elav>ampk*^{T184D} = 43.9±3.1, *trpml*^{1} = 46.0±2.3, *elav>ampk*^{T184D}*;trpml*^{1} = 46.4±1.7, *UAS-ampk*^{K56R}*;trpml*^{1} = 46.3±2.1, *elav>ampk*^{K56R}*;trpml*^{1} = 53.4±3.3; *, p =3.3x10^{-14}, ANOVA; n = 10-18 NMJs per genotype.

Figure S1D Number of boutons: *UAS-S6K*^{KQ} = 65.1±2.2, *elav>S6K*^{KQ} = 68.4±5.0, *UAS-thor* = 61.6±1.9, *elav>thor* = 66.2±2.8; n = 8-16 NMJs per genotype.

Figure S1E Number of boutons: DMSO control = 70.5±4.4, 1 µM rapamycin = 78.2±4.8; n = 10-12 NMJs per genotype.

Figure S1B Relative pMAD intensities (normalized to WT mean): WT = 1±0.02, *trpml*^{1} = 0.75±0.1; p = 0.09, unpaired Student's t-test, n = 5-6 NMJs per genotype.

Figure S1D Relative pMAD intensities (normalized to WT mean): WT = 1±0.09, *trpml*^{1} = 1.2±0.13; n = 4 animals per genotype.

Figure S1E Relative Wg intensities (normalized to WT mean): WT = 1±0.2, *trpml*^{1} = 1.1±0.35; n = 3-6 NMJs per genotype.

Figure S4B Relative pJNK/JNK levels: control = 1±0.004, chloroquine fed larvae = 0.69±0.09; *, p = 0.04, unpaired Student's t-test, n = 3 independent samples per condition.

Figure S4G Number of boutons: *hiw*^{ND8}*; UAS-cln3*^{IR} = 113.5±4.8, *hiw*^{ND8}*; ok371-GAL4* = 113.7±5.0, *hiw*^{ND8}*; ok371>cln3*^{IR} = 95.5±3.4; *, p = 0.02, ANOVA; n = 6-19 NMJs per genotype.

Figure S4M Relative pAkt^{S473} levels normalized to control: CH5424802 treated larvae = 0.8±0.05; *, p = 0.01, paired Student's t-test, n = 5 pairs of independent samples per condition.

Supplemental References

Barcelo, H., and Stewart, M.J. (2002). Altering Drosophila S6 kinase activity is consistent with a role for S6 kinase in growth. Genesis *34*, 83-85.

Brand, A.H., and Perrimon, N. (1993). Targeted gene expression as a means of altering cell fates and generating dominant phenotypes. Development *118*, 401-415.

Budnik, V. (1996). Synapse maturation and structural plasticity at Drosophila neuromuscular junctions. Curr Opin Neurobiol *6*, 858-867.

Collins, C.A., Wairkar, Y.P., Johnson, S.L., and DiAntonio, A. (2006). Highwire restrains synaptic growth by attenuating a MAP kinase signal. Neuron *51*, 57-69.

Hennig, K.M., Colombani, J., and Neufeld, T.P. (2006). TOR coordinates bulk and targeted endocytosis in the *Drosophila melanogaster* fat body to regulate cell growth. J Cell Biol *173*, 963-974.

Kim, E., Goraksha-Hicks, P., Li, L., Neufeld, T.P., and Guan, K.L. (2008). Regulation of TORC1 by Rag GTPases in nutrient response. Nat Cell Biol *10*, 935-945.

Kockel, L., Kerr, K.S., Melnick, M., Bruckner, K., Hebrok, M., and Perrimon, N. (2010). Dynamic switch of negative feedback regulation in Drosophila Akt-TOR signaling. PLoS Genet *6*, e1000990.

Lee, G., and Chung, J. (2007). Discrete functions of rictor and raptor in cell growth regulation in Drosophila. Biochem Biophys Res Commun *357*, 1154-1159.

Lin, D.M., and Goodman, C.S. (1994). Ectopic and increased expression of Fasciclin II alters motoneuron growth cone guidance. Neuron *13*, 507-523.

Martin-Blanco, E., Gampel, A., Ring, J., Virdee, K., Kirov, N., Tolkovsky, A.M., and Martinez-Arias, A. (1998). puckered encodes a phosphatase that mediates a feedback loop regulating JNK activity during dorsal closure in Drosophila. Genes Dev *12*, 557-570.

Meyer, F., and Aberle, H. (2006). At the next stop sign turn right: the metalloprotease Tolloid-related 1 controls defasciculation of motor axons in Drosophila. Development *133*, 4035-4044.

Natarajan, R., Trivedi-Vyas, D., and Wairkar, Y.P. (2013). Tuberous sclerosis complex regulates Drosophila neuromuscular junction growth via the TORC2/Akt pathway. Hum Mol Genet *22*, 2010-2023.

Pauli, A., Althoff, F., Oliveira, R.A., Heidmann, S., Schuldiner, O., Lehner, C.F., Dickson, B.J., and Nasmyth, K. (2008). Cell-type-specific TEV protease cleavage reveals cohesin functions in Drosophila neurons. Dev Cell *14*, 239-251.

Pulipparacharuvil, S., Akbar, M.A., Ray, S., Sevrioukov, E.A., Haberman, A.S., Rohrer, J., and Krämer, H. (2005). *Drosophila* Vps16A is required for trafficking to lysosomes and biogenesis of pigment granules. J Cell Sci *118*, 3663-3673.

Ranganayakulu, G., Schulz, R.A., and Olson, E.N. (1996). Wingless signaling induces nautilus expression in the ventral mesoderm of the Drosophila embryo. Dev Biol *176*, 143-148.

Sluss, H.K., Han, Z., Barrett, T., Goberdhan, D.C., Wilson, C., Davis, R.J., and Ip, Y.T. (1996). A JNK signal transduction pathway that mediates morphogenesis and an immune response in Drosophila. Genes Dev *10*, 2745-2758.

Stocker, H., Radimerski, T., Schindelholz, B., Wittwer, F., Belawat, P., Daram, P., Breuer, S., Thomas, G., and Hafen, E. (2003). Rheb is an essential regulator of S6K in controlling cell growth in Drosophila. Nat Cell Biol *5*, 559-565.

Sweeney, S.T., and Davis, G.W. (2002). Unrestricted synaptic growth in *spinster*-a late endosomal protein implicated in TGF-β-mediated synaptic growth regulation. Neuron *36*, 403-416.

Venkatachalam, K., Long, A.A., Elsaesser, R., Nikolaeva, D., Broadie, K., and Montell, C. (2008). Motor deficit in a *Drosophila* model of mucolipidosis type IV due to defective clearance of apoptotic cells. Cell *135*, 838-851.

Wan, H.I., DiAntonio, A., Fetter, R.D., Bergstrom, K., Strauss, R., and Goodman, C.S. (2000). Highwire regulates synaptic growth in Drosophila. Neuron *26*, 313-329.

Wong, C.O., Li, R., Montell, C., and Venkatachalam, K. (2012). Drosophila TRPML Is Required for TORC1 Activation. Curr Biol *22*, 1616-1621.

Wu, C., Wairkar, Y.P., Collins, C.A., and DiAntonio, A. (2005). Highwire function at the Drosophila neuromuscular junction: spatial, structural, and temporal requirements. J Neurosci *25*, 9557-9566.

Yip, C.K., Murata, K., Walz, T., Sabatini, D.M., and Kang, S.A. (2010). Structure of the human mTOR complex I and its implications for rapamycin inhibition. Mol Cell *38*, 768-774.

Figure S1 (related to Figure 2)

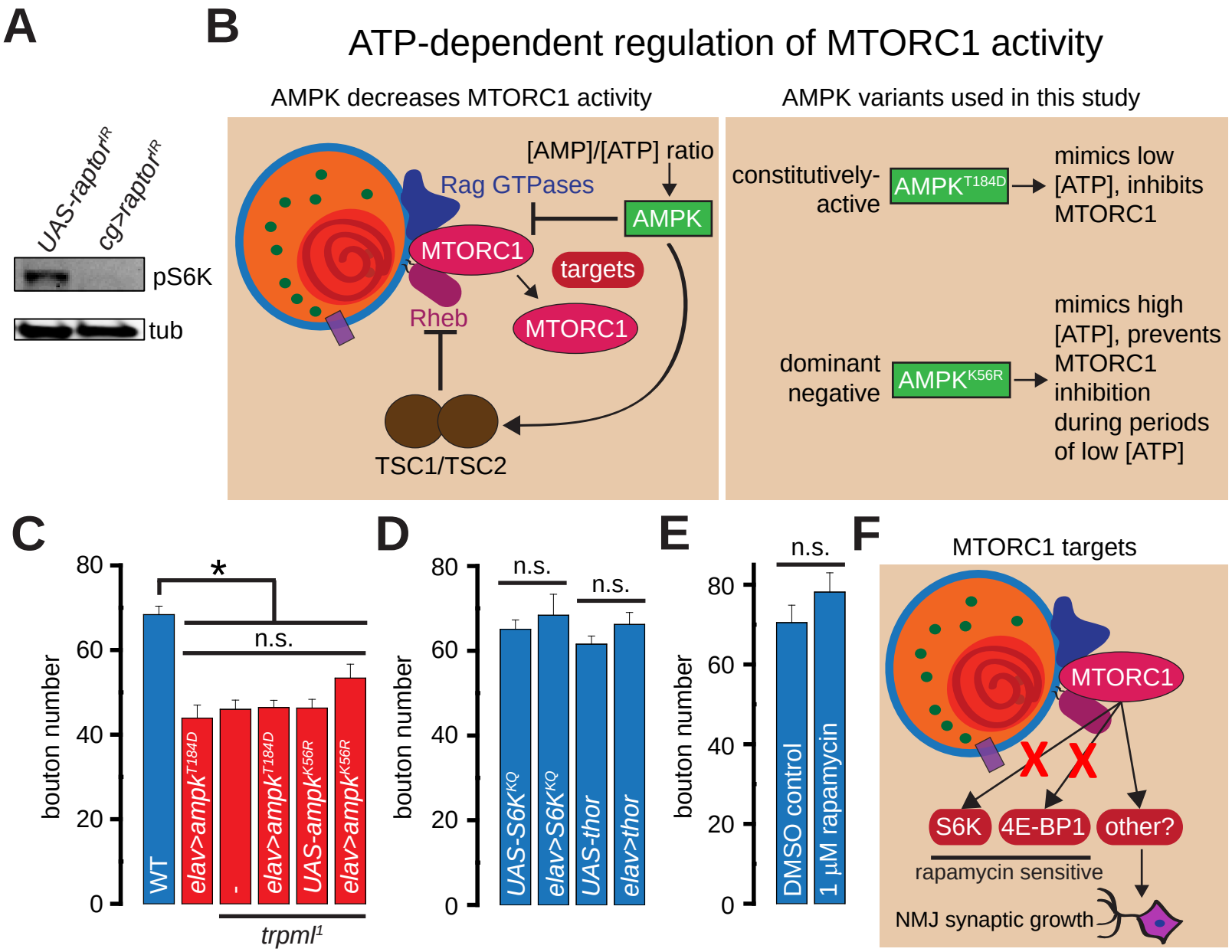

Figure S1. Synaptic growth defects following lysosomal dysfunction do not arise from elevated AMPK activity or diminished phosphorylation of S6K/Thor.

(A) Western blots performed *Drosophila* 3rd instar larval fat-body from animals of the indicated genotypes probed with α-pS6K and α-tubulin primary antibodies.

(B) Schematic diagram showing the role of AMPK in regulating MTORC1 activity and the AMPK variants used in this study.

(C-D) Bar graphs showing the average bouton numbers in animals of the indicated genotypes.

(E) Bar graph showing the average number of boutons in wild-type larvae reared on instant food containing the indicated drugs.

(F) Schematic showing that MTORC1 regulates NMJ synaptic growth via targets other than S6K and 4E-BP1.

All values represent mean ±SEM, and "*" represents statistical significance. Please consult the *Supporting Information* for all values and information on statistical tests employed. Abbreviations: n.s., not significant.

Figure S2 (related to Figure 3)

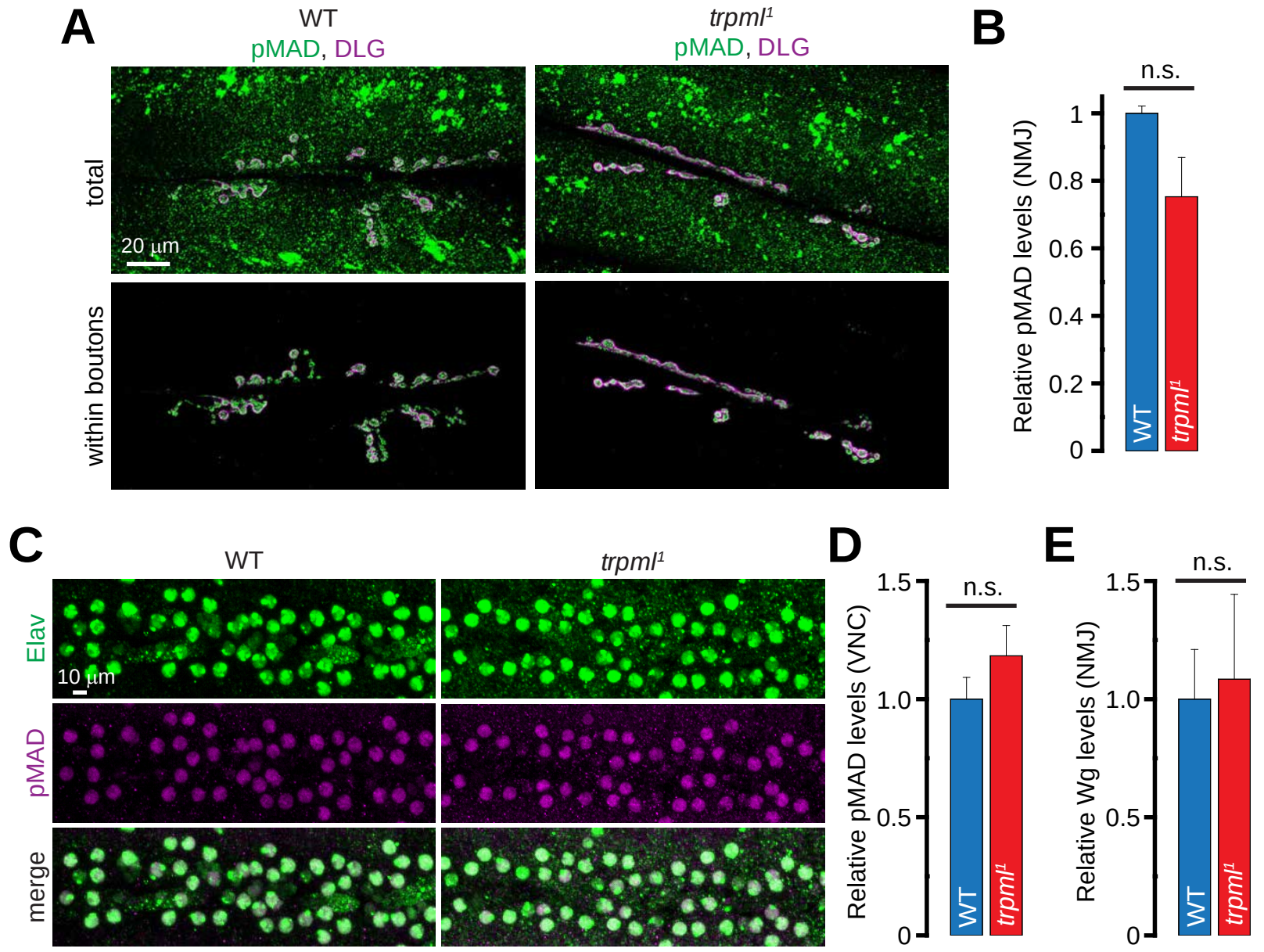

Figure S2. Synaptic growth defects following lysosomal dysfunction do not arise from alterations in BMP/TGF-β signaling or Wg release.

(A) Confocal images of 3rd instar larval NMJs from animals of the indicated genotypes stained with antibodies against pMAD (green) and DLG (magenta). Scale bar shown in top-left panel also applies to remaining panels. Please refer to the *Experimental Procedures* for information on the approach utilized to isolate the pMAD signal within boutons.

(B) Bar graph showing the relative pMAD intensities normalized to the Eps15 intensities within NMJ boutons in animals of the indicated genotypes. All values were normalized to the Eps15 staining intensities.

(C) Confocal images of 3rd instar larval VNC from animals of the indicated genotypes stained with antibodies against pMAD (magenta) and Elav (green). Scale bar shown in top-left panel also applies to remaining panels.

(D) Bar graph showing the relative pMAD intensities normalized to the Elav intensities within VNC in animals of the indicated genotypes.

(E) Bar graphs showing the relative Wg intensities normalized to the Eps15 intensities within NMJ boutons in animals of the indicated genotypes. All values were normalized to the Eps15 staining intensities. Please refer to the *Experimental Procedures* for information on the approach utilized to isolate the Wg signal within boutons.

All values represent mean ±SEM. Please consult the *Supporting Information* for all values and information on statistical tests employed. Abbreviations: n.s., not significant.

Figure S3 (related to Figure 5)

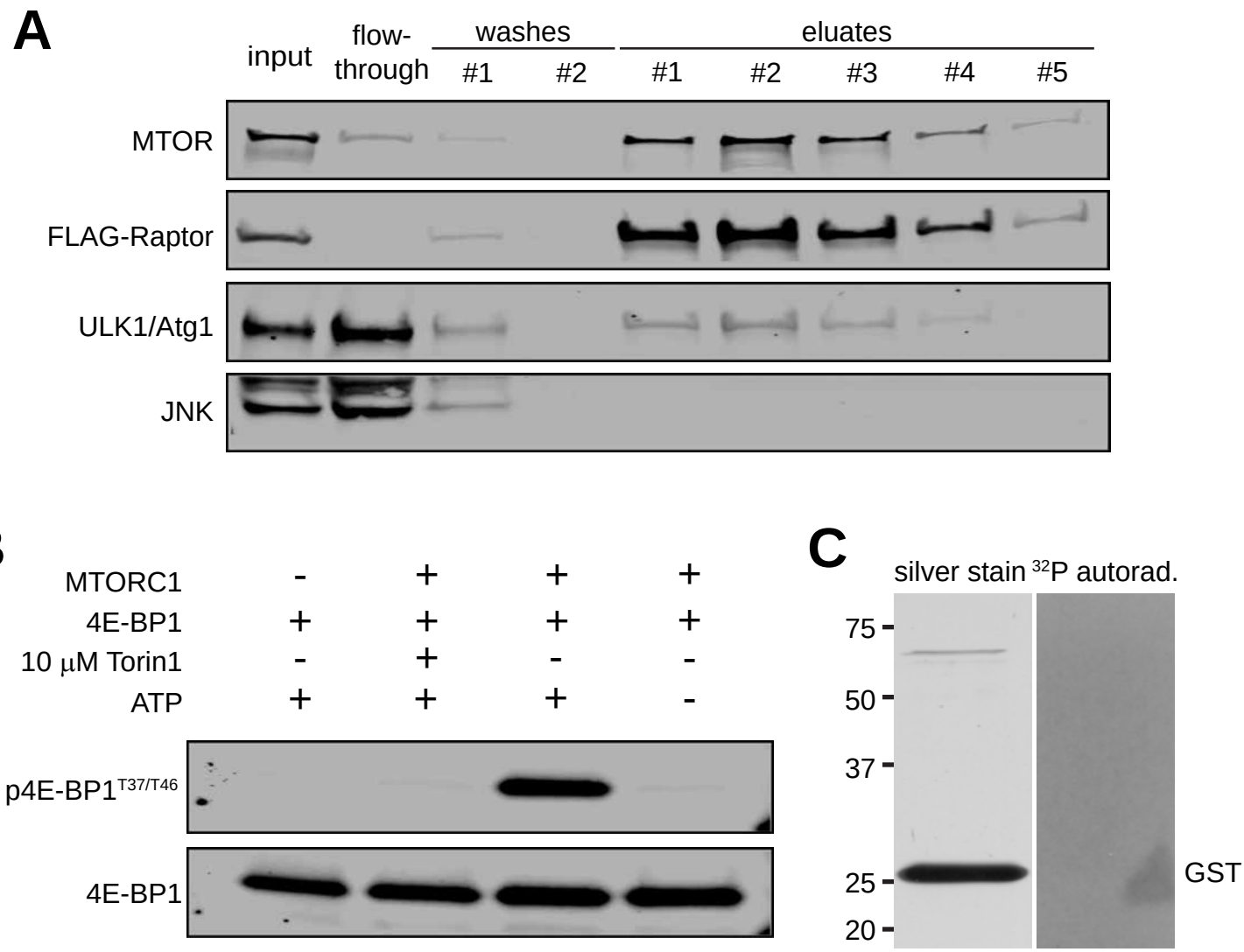

Figure S3. Characterization of purified MTORC1

(A) Western blot performed on the indicated fractions from the FLAG-Raptor purification probed with antibodies against MTOR, FLAG, ULK1/Atg1 and JNK.

(B) *In vitro* kinase assay using purified MTORC1 on recombinant 4E-BP1. Upper panel shows that 4E-BP1 is phosphorylated only in the presence of MTORC1 and ATP, and this phosphorylation of 4E-BP1 is inhibited by 10 μM Torin1. Lower panel shows total 4E-BP1 in all the lanes.

(C) *In vitro* kinase assay using purified MTORC1 on recombinant GST. Left panel, silver stain showing the presence of GST. Right panel, ^{32}P autoradiogram showing that GST is not phosphorylated by MTORC1.

Figure S4 (related to Figures 6 and 7)

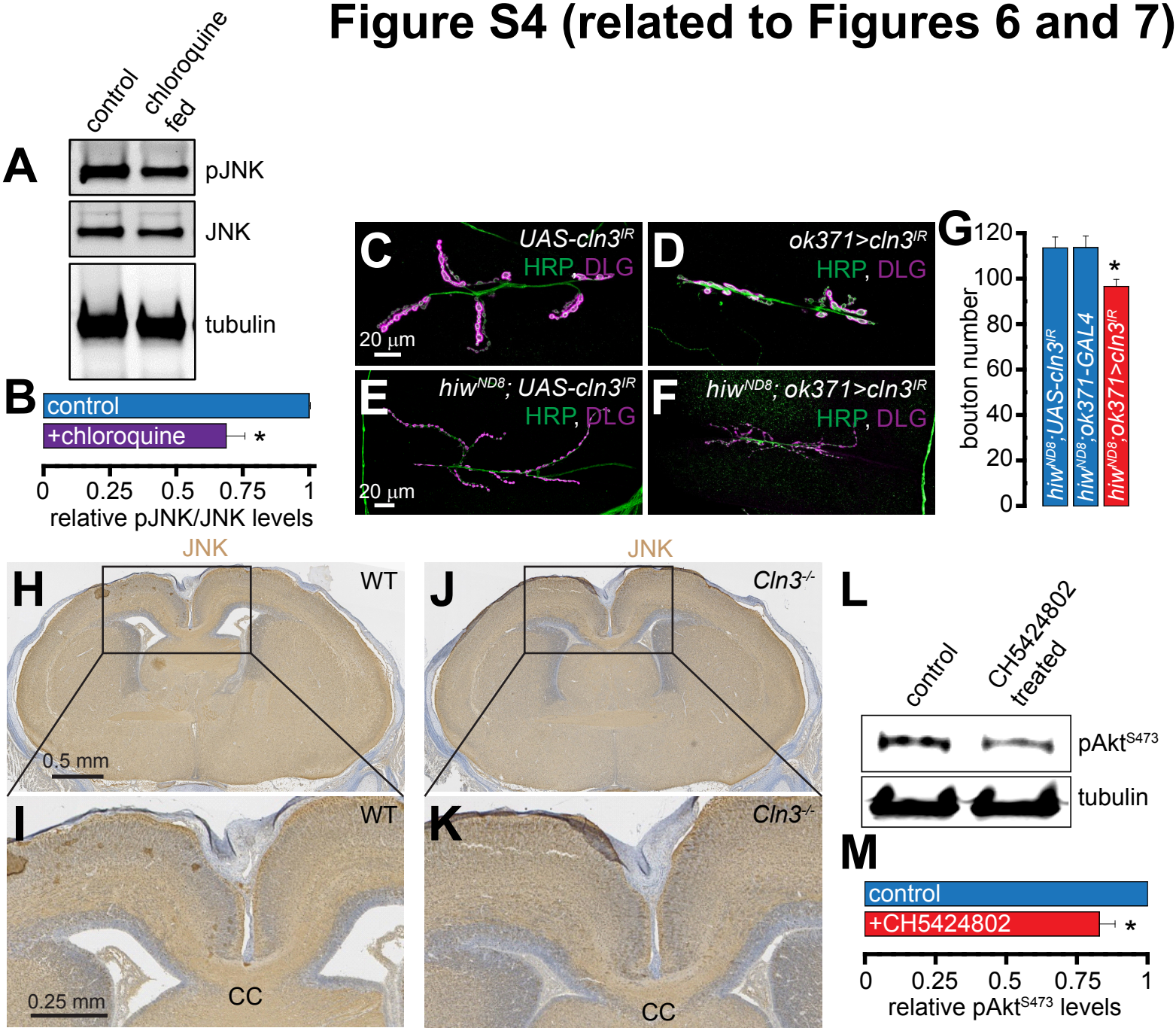

Figure S4.

(A) Western blots performed on 3rd instar larval brain extracts derived from control or choloroquine fed larvae probed with α-pJNK, α-JNK, and α-tubulin primary antibodies.

(B) Bar graph showing the relative pJNK/JNK levels in 3rd instar larval brain extracts derived from control or choloroquine fed larvae.

(C-F) Confocal images of 3rd instar larval NMJs from animals of the indicated genotypes stained with antibodies against HRP (green) and DLG (magenta). Scale bar shown in (C) and (E) also apply to (D) and (F) respectively.

(G) Bar graph showing the average bouton numbers in animals of the indicated genotypes.

(H and J) Coronal sections of E19.5 mouse brains of the indicated genotypes showing α-JNK staining by immunohistochemistry. Scale bar shown in (F) also applies to (H).

(Iand K) Higher magnification of the boxed regions from (F) and (H) respectively.

(L) Western blots performed on 3rd instar larval brain extracts derived from tissues treated with DMSO (control) or CH5424802 probed with α-pAkt^{S473} and α-tubulin primary antibodies.

(M) Bar graph showing the relative pAktS^{473} levels in 3rd instar larval brain extracts derived from tissues treated with DMSO (control) or CH5424802 (1 μM) for 1 hour.

All values represent mean ±SEM, and "*" represents statistical significance. Please consult the *Supporting Information* for all values and information on statistical tests employed. Abbreviations: CC, corpus callosum.